

Part 4—Spectroscopy, Kinetics, and Quantum Chemistry of
Alkoxy Isomerization

Part of the work presented in Part 4 of this thesis (Chapters 7 and 8) has been published in our paper on the cavity ringdown spectroscopy and kinetics of alkoxy isomerization. Reproduced in part with permission from Sprague et al.³¹ Copyright 2012 American Chemical Society.

Chapter 7—Direct Detection of Primary Products of Alkoxy Isomerization: The OH Stretch Spectra of δ -HOC₄H₈•, δ -HOC₄H₈OO•, δ -HO-1-C₅H₁₀•, and δ -HO-1-C₅H₁₀OO•

Abstract

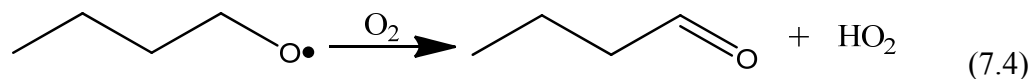
The primary products of *n*-butoxy and 2-pentoxy isomerization in the presence and absence of O₂ have been detected using Pulsed Laser Photolysis-Cavity Ringdown Spectroscopy (PLP-CRDS). Alkoxy radicals were generated by photolysis of alkyl nitrite precursors (*n*-butyl nitrite or 2-pentyl nitrite), and the isomerization products were detected by infrared cavity ringdown spectroscopy 20 μ s after the photolysis. We report the mid-IR OH stretch (ν_1) absorption spectra for δ -HOC₄H₈•, δ -HOC₄H₈OO•, δ -HO-1-C₅H₁₀•, and δ -HO-1-C₅H₁₀OO•. The observed ν_1 bands are similar in position and shape to their parent alcohols (*n*-butanol and 2-pentanol), although the HOROO• absorption is somewhat stronger than the HOR• absorption. We observe that these ν_1 spectra are constant over at least 800 μ s, indicating that secondary products have similar spectra to our primary products. We show here that the ν_1 spectra can be used to make relative rate measurements of alkoxy isomerization to reaction with O₂ (larger data sets in Chapter 8). We also report the thermodynamic properties of 2-pentyl nitrite ($p_{\text{vap}}(T)$, $\Delta_{\text{vap}}H$, and $T_{\text{boil,1atm}}$).

Introduction

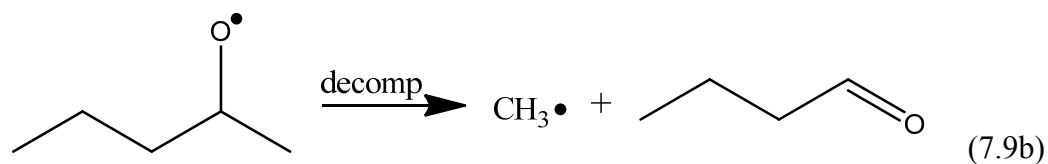
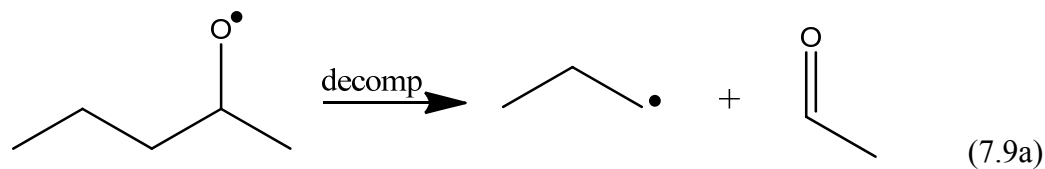
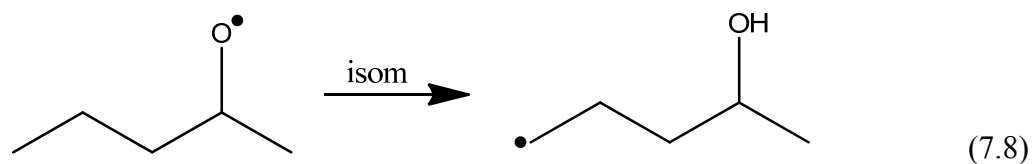
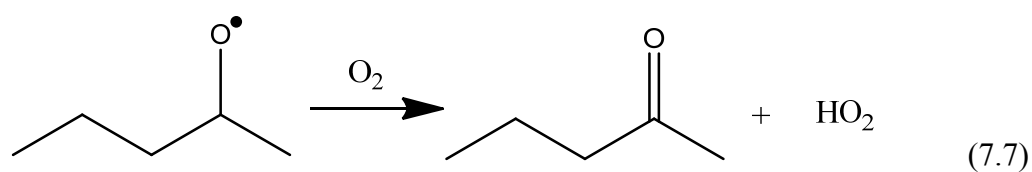
Alkoxy radicals (RO•) are an important intermediate species in the oxidation of volatile organic hydrocarbons through the HO_x and NO_x cycles in the atmosphere. Alkoxy radicals are formed predominantly by a chain of three reactions: first oxidation of a hydrocarbon with OH to form an alkyl radical (Reaction 7.1), immediate association with O₂ to form an alkyl peroxy radical (Reaction 7.2), then finally reaction of alkyl peroxy radicals with NO to form the alkoxy radical (Reaction 7.3).¹⁻³



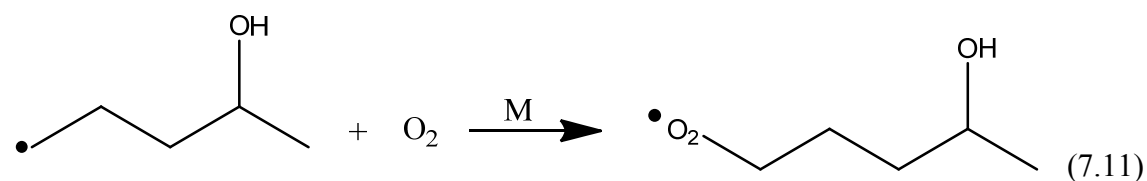
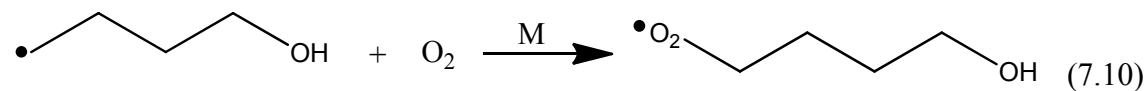
The alkoxy radicals react further via one of three mechanisms: α -hydrogen abstraction by O₂ to form a carbonyl and HO₂, unimolecular isomerization involving a 1,5-hydrogen shift via a cyclic transition state, or unimolecular dissociation via β -scission. These three reactions for the *n*-butoxy radical (a primary alkoxy radical) and the 2-pentoxy radical (a secondary alkoxy radical) are shown below.

n-butoxy:

2-pentoxy:



In the presence of O_2 , the δ -hydroxyalkyl radicals formed in Reactions 7.5 and 7.8 rapidly associate with O_2 to form δ -hydroxyalkylperoxy radicals, Reactions 7.10 and 7.11.



The computed energetics for the reactions of the *n*-butoxy radical are shown in Figure 7.1. The diagram is a composite of two different calculations; numerous *ab initio* calculations have been performed to calculate the energetics and RRKM reaction rates for decomposition and isomerization of alkoxy radicals,¹²⁹⁻¹⁴⁰ but very few calculations have been performed on the reaction with O₂.^{131, 133, 141} For the *n*-butoxy radical, Somnitz and Zellner^{136, 138} calculated barriers for decomposition and isomerization of 15.0 kcal mol⁻¹ and 10.2 kcal mol⁻¹, respectively, at the modified G2(MP2,SVP) level of theory. Jungkamp et al.¹³¹ calculate a barrier for reaction with O₂ of 8.2 kcal mol⁻¹, at the B3LYP/6-311+G(3df,2p)//B3LYP/6-31G(d,p) level of theory.

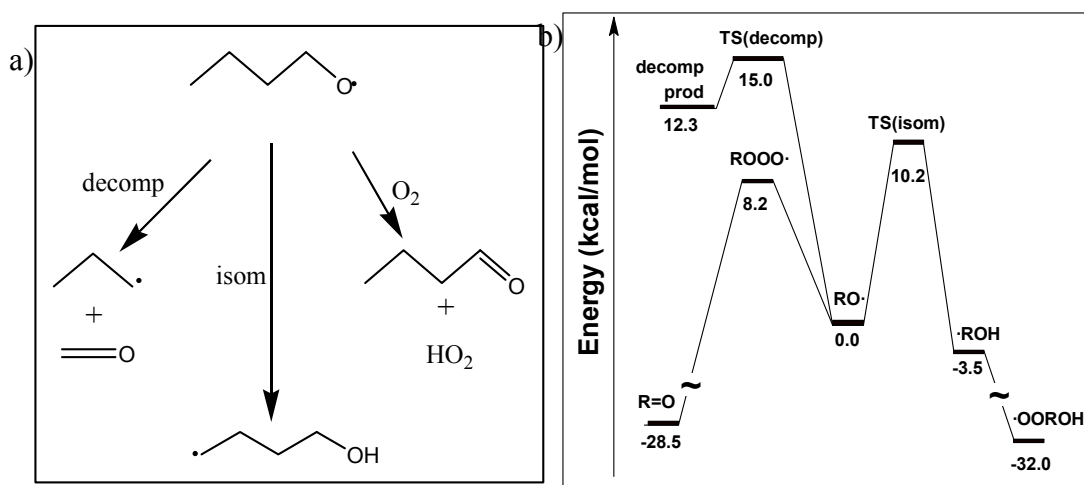


Figure 7.1. Reaction map (a) and energy diagram (b) for the decomposition, reaction with O₂, and isomerization reactions of alkoxy radicals. The energies listed are for *n*-butoxy. Energies for the isomerization and decomposition are taken from Somnitz and Zellner^{138, 139} at the modified G2(MP2,SVP) level of theory, while energies for the reaction with O₂ are taken from Jungkamp et al.¹³¹ at the B3LYP/6-311+G(3df,2p)//B3LYP/6-31G(d,p) level of theory. All energies listed are relative to the *n*-butoxy radical. Reprinted with permission from Sprague et al.³¹ Copyright 2012 American Chemical Society.

Many experimental and theoretical studies have shown that relative importance of the reaction pathways of alkoxy radicals depends critically upon the structure of the

alkoxy radical. Several reviews are available.^{118, 130, 142-144} For all alkoxy radicals, unimolecular decomposition is an available pathway, and the rate of decomposition is faster when the transition state is stabilized through substitution at the α - or β -carbon. Those alkoxy radicals containing an α -hydrogen can also undergo hydrogen abstraction reaction with O₂. Only radicals which can form a 6-membered ring transition state have a sufficiently low barrier for unimolecular isomerization to be atmospherically relevant,^{142, 145-148} and the isomerization rate is fastest when the product is a secondary or tertiary alkyl radical.¹⁴² For molecules in which all three pathways are possible, isomerization and reaction with O₂ dominate under atmospheric conditions. Measurements of k_{O_2} have generally yielded values within a factor of two of $1 \times 10^{-14} \text{ cm}^3 \text{ molec}^{-1} \text{ s}^{-1}$ at 298 K, with small dependencies on temperature and the structure of the alkoxy radical.^{143, 144} Variations in k_{isom} and k_{decomp} with pressure, temperature, and molecular structure are much larger, spanning many orders of magnitude because of the significant barriers involved and differences in the densities of states.^{129, 134, 135, 137, 139, 140, 149-152}

Isomerization has been a particularly difficult process to study experimentally due to the wide range of values of k_{isom} and fast secondary chemistry. In molecules which can form a 6-membered ring, isomerization generally occurs on the timescale of microseconds or less. In addition, the primary products of isomerization are hydroxyalkyl radicals with fast secondary reaction rates. As a result, the isomerization of alkoxy radicals has not yet been observed directly. Many previous studies of k_{isom} have focused on the simplest alkoxy radicals that can undergo isomerization: *n*-butoxy, 1-pentoxy, and 2-pentoxy. Under conditions relevant to the lower atmosphere (300 K, 1 bar, 21% O₂) the lifetime for reaction with O₂ is on the order 20 μs .²⁸ Previous relative rate

measurements have estimated the lifetimes for isomerization under these conditions to be on the order of 3 μs for Reaction 7.5 and shorter for Reaction 7.8.²⁸ The decomposition reactions have been estimated to occur on longer timescales: on the order 1 ms for Reaction 7.6 and 100 μs for Reaction 7.9. As a result, isomerization and reaction with O_2 are expected to be the dominant fates for these alkoxy radicals.

Most of the previous experimental work^{146, 148, 153-158} has measured the branching ratio of the isomerization and O_2 reaction channels, $k_{\text{isom}}/k_{\text{O}_2}$ by end-product analysis. Typically, butanal is detected, and a kinetics model is used to back out the relevant rate constants. Hein et al.¹⁵⁹ obtain an absolute value for k_{isom} by measuring the disappearance of OH and NO_2 . The resulting data are then fit to a kinetics model to back out k_{isom} . Although the majority of studies are in good agreement with each other (Table 7.1), it is possible for errors in the kinetics models to systematically affect all of the reported $k_{\text{isom}}/k_{\text{O}_2}$. Most of these prior experiments have included NO. In this case, the products of Reactions 7.10 and 7.11 react with NO via Reaction 7.3 to generate a secondary alkoxy radical. This secondary alkoxy radical can also undergo reaction via several pathways, leading to a large variety of possible end-products. Often, several reaction pathways can generate the same products, and so it can be difficult to deduce reaction mechanisms by relying on end-product data.¹³¹

Table 7.1. Comparison of previous relative rate constant determinations $k_{\text{isom}}/k_{\text{O}_2}$ and derived k_{isom} for *n*-butoxy and 2-pentoxy

	$k_{\text{isom}}/k_{\text{O}_2}$ (10^{19} cm^{-3}) ^a	k_{isom} (10^5 s^{-1}) ^b	Molecules detected	Method	<i>P</i> (<i>torr</i>)	Ref
<i>n</i>-butoxy	2.0 ± 0.4	2.7 ± 1.5	Butyl nitrite, Butanal,	Static, FTIR	700	Cassanelli ¹⁵⁵
	1.5 ± 0.4	2.1 ± 1.2	4-hydroxy butanal	Static, GC	760	Cox ¹⁵⁶
	1.9 ± 0.4	2.7 ± 1.4	Butane, Butanal	Static, FTIR	700	Niki ¹⁴⁸
	2.1 ± 0.5	2.9 ± 1.6	Butyl nitrite, Butanal	Slow flow, GC	760	Cassanelli ¹⁶⁰
	1.8 ± 1.1	2.5 ± 2.0	Butyl nitrite, Butanal	Slow flow, GC	760	Cassanelli ¹⁶⁰
	1.8 ± 0.6	2.5 ± 1.5	Butane, Butanal	Static, FTIR	760	Geiger ¹⁶¹
	0.25 ± 0.19 ^c	0.35 ± 0.20 ^c	Butanal, 4-hydroxy butanal	Fast flow, LIF	38	Hein ¹⁵⁹
	1.6	2.2	OH and NO ₂	Static, GC	740	Carter ¹⁵⁴
	2.1 ± 1.8 ^d	2.9 ± 1.4 ^d		Recommendation	760	IUPAC ¹¹⁸
2-pentoxy	3.1 ^e	2.5 ^e	2-pentanone	Static, GC	700	Atkinson ¹⁴⁵
	0.15	0.12 ^f	Acetone, Acetaldehyde, 2-hexanol	Static, GC	760	Dóbé ¹⁵⁷

a) All uncertainties are 2σ. All studies other than the current work treat all alkoxy reactions besides isomerization and reaction with O₂ as negligible.

b) Computed k_{isom} assuming literature value of $k_{\text{O}_2} = (1.4 \pm 0.7) \times 10^{-14} \text{ cm}^3 \text{ s}^{-1}$ for *n*-butoxy,²⁸ and $k_{\text{O}_2} = 8 \times 10^{-15} \text{ cm}^3 \text{ s}^{-1}$ for 2-pentoxy (no estimate available for the uncertainty).¹⁴²

c) Unlike the other studies, Hein directly measured k_{isom} . In this table, we calculate the ratio $k_{\text{isom}}/k_{\text{O}_2}$ from Hein's measurement using the literature value of k_{O_2} .

d) The IUPAC recommendation for $k_{\text{isom}}/k_{\text{O}_2}$ is computed from their individual recommendations of the isomerization and O₂ reactions

e) The uncertainty on $k_{\text{isom}}/k_{\text{O}_2}$ is reported by Atkinson as a factor of 2.

f) Dóbé's study calculates k_{isom} from the relative rate $k_{\text{isom}}/k_{\text{decomp}}$ and their measured rate $k_{\text{decomp}} = 1.2 \times 10^4 \text{ s}^{-1}$. The $k_{\text{isom}}/k_{\text{O}_2}$ reported in this table uses the literature value of $k_{\text{O}_2} = 8 \times 10^{-15} \text{ cm}^3 \text{ s}^{-1}$ for 2-pentoxy.¹⁴²

A better method for studying alkoxy chemistry is to directly detect the species involved in the primary reactions of alkoxy chemistry (Reactions 7.4–7.11). Such methods avoid the need for assumptions about secondary chemistry, and should lead to reduced uncertainty on the kinetic rate constants. Numerous spectroscopic studies on the alkoxy radicals themselves have been carried out, typically employing laser-induced fluorescence (LIF) to measure the A-X or B-X electronic transitions.¹⁶²⁻¹⁸² However, fluorescence is quenched for larger alkoxy radicals due to internal conversion, making LIF experiments inappropriate for studying the larger alkoxy radicals that can isomerize.

The approach previously taken in our laboratory has been direct detection of the primary isomerization products, HOR• (formed in Reactions 7.5 and 7.8), and HOROO• (Reactions 7.10 and 7.11), via the ν_1 (OH stretch) cavity ringdown spectra.^{29, 30} Measuring the ν_1 intensity as a function of $[O_2]$ will show how the isomerization reactions compete with the O_2 reactions. In principle, it should be possible to obtain clean ν_1 spectra of HOR• and HOROO• for appropriate experimental conditions (radical concentrations, timing of measurement). Careless choices of these conditions (very high radical concentrations, very long times after initial alkoxy radical generation) will lead to detection of a variety of secondary products with their own OH stretch spectra. Besides the fact that the reported spectra are not truly HOR• or HOROO•, the relative kinetics measurements may or may not be accurate if the ratios of secondary products change with $[O_2]$. By reducing radical concentrations and time after alkoxy generation, we can obtain cleaner spectra than previous experiments in our group were able to.

In this thesis chapter, we report the first clean OH stretch spectra of δ -HOC₄H₈•, δ -HOC₄H₈OO•, δ -HO-1-C₅H₁₀•, and δ -HO-1-C₅H₁₀OO•. Compared to the previous experiments performed by Garland and Mollner,^{29, 30} here we make use of shorter timescales, lower $[RO\bullet]$, and lower $[O_2]$ to obtain cleaner spectra. Similar to Garland and Mollner's previous experiments, HOR• and HOROO• (R = C₄H₈ or C₅H₁₀) were generated through pulsed laser photolysis of *n*-butyl nitrite or 2-pentyl nitrite in the absence or presence of O₂. Cavity ringdown spectroscopy was used to measure the resulting spectrum over the range 3610-3720 cm⁻¹, 20 μ s after photolysis. Additional spectra were recorded 800 μ s after photolysis in order to assess how the OH stretch peak changes as secondary chemistry proceeds, allowing us to determine the effects of

secondary chemistry on Garland and Mollner's experiments. The OH stretch peak heights were also measured as a function of $[O_2]$ to obtain k_{isom}/k_{O_2} , allowing us to determine if the previous measurements were affected by the mixture of products that were actually being detected.

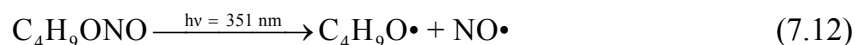
Methods

Apparatus and Chemicals

The cavity ringdown spectrometer, laser system, and gas kinetics flow cell have been described in detail in Chapter 2 (Figures 2.5, 2.7, 2.8). Briefly, the tunable near-infrared light used to measure the spectrum was generated using an optical parametric amplifier. For 65 mJ of 532 nm light and 4–12 mJ of tunable red light (620–665 nm), 0.6–0.8 mJ of tunable infrared light was generated ($2900\text{--}3800\text{ cm}^{-1}$). The infrared light was sent into an optical cavity consisting of two highly reflective mirrors (Los Gatos Research, 2.8 μm peak, $R = 99.98\%$). Ringdown traces were collected with a liquid nitrogen cooled InSb detector (Judson J10D-M204-R01M-60) connected to a voltage amplifier (Analog Modules 351A-3) and PC oscilloscope card (GageScope CS1450). 80 μs of ringdown data were collected per shot, and 16 ringdowns were collected and averaged before being fit. The first eighth of the ringdown lifetime was removed before the data were refit in order to eliminate errors caused from noise near the peak of the ringdown.

The δ -hydroxybutylperoxy radicals were formed by photolysis of *n*-butyl nitrite (95%, Sigma-Aldrich) in the presence of O_2 (Reactions 7.12, 7.5, and 7.10). Photolysis was initiated by 351 nm light from the excimer laser described in Chapter 2. Typical UV

flux was kept at 1.8×10^{17} photons cm^{-2} . The absorption cross section of *n*-butyl nitrite at 351 nm is $\sigma_{351\text{nm}} = 8.0 \times 10^{-20}$ $\text{cm}^2 \text{molec}^{-1}$,³² resulting in 1.5% of the alkyl nitrite being photolyzed.



n-butyl nitrite was introduced to the gas kinetics cell by flowing N_2 gas through a bubbler kept at 0 °C. Prior to usage, the *n*-butyl nitrite went through a minimum of three freeze-pump-thaw cycles in order to degas the sample of oxygen and to reduce the concentration of impurities (such as NO, nitrous oxides, aldehydes, and acids). Briefly, one cycle consists of freezing the nitrite in liquid nitrogen, vacuum pumping on the sample for 10–20 minutes, then isolating the sample and thawing. The gas bubbles that evolve represent impurities that have a higher vapor pressure than the nitrite. Cycles were repeated until minimal to no gas evolved during thawing.

The δ -hydroxy-1-pentylperoxy radicals were formed by photolysis of 2-pentyl nitrite in the presence of O_2 , similar to the chemistry for the *n*-butoxy system presented above. However, 2-pentyl nitrite is not commercially available, requiring us to synthesize the 2-pentyl nitrite according to standard protocol.¹⁸³ The synthesis was first performed on a small scale (listed chemical quantities) to verify the formation of 2-pentyl nitrite before scaling up. 22 g of NaNO_2 was dissolved in 88 mL of H_2O , and cooled to -5 °C. A mixture of 6 mL H_2O , 8.5 mL concentrated H_2SO_4 , and 33 mL of 2-pentanol was cooled to -5°C and added drop wise to the NaNO_2 solution over the course of 60 minutes. Solid Na_2SO_4 was filtered, and the upper layer containing 2-pentyl nitrite was separated. The

crude product was vacuum distilled at 30 torr to remove water and excess pentanol. Based on FTIR spectra of the 2-pentyl nitrite (shown in the *Results* section), $[\text{RONO}]:[\text{ROH}] = 24$, $[\text{RONO}]:[\text{NO}] = 240$, and $[\text{RONO}]:[\text{H}_2\text{O}] = 14$ (overall purity 90%). Approximately 15 mL of distilled 2-pentyl nitrite was yielded. After FTIR characterization, two batches of 2-pentyl nitrite (150 mL each) were synthesized: one for the CRDS experiment, and one to measure thermodynamic properties of 2-pentyl nitrite.

Quantum chemistry calculations suggest that $\sigma_{351\text{nm}}(\text{C}_5\text{H}_{11}\text{ONO}) = 0.75 \times \sigma_{351\text{nm}}(\text{C}_4\text{H}_9\text{ONO})$, or $6.0 \times 10^{-20} \text{ cm}^2 \text{ molec}^{-1}$. For a photolysis flux of 2.0×10^{17} photons cm^{-2} , 1.2% of the pentyl nitrite is photolyzed.

Experimental and Flow Conditions

The majority of the $\delta\text{-HOC}_4\text{H}_8\bullet$, $\delta\text{-HOC}_4\text{H}_8\text{OO}\bullet$, $\delta\text{-HO-1-C}_5\text{H}_{10}\bullet$, and $\delta\text{-HO-1-C}_5\text{H}_{10}\text{OO}\bullet$ spectra were acquired at a single set of conditions for each species in order to provide for signal averaging. The main difference between the conditions required for detection of the two species is that detections of $\delta\text{-HOC}_4\text{H}_8\bullet$ and $\delta\text{-HO-1-C}_5\text{H}_{10}\bullet$ were made at $[\text{O}_2] = 0$, while detections of $\delta\text{-HOC}_4\text{H}_8\text{OO}\bullet$ and $\delta\text{-HO-1-C}_5\text{H}_{10}\text{OO}\bullet$ were made at $[\text{O}_2] = 9 \times 10^{17} \text{ molec cm}^{-3}$. The spectra of both species were measured by scanning across a range of frequencies (3610-3720 cm^{-1} , step size 0.2 cm^{-1}) while at a constant time after photolysis of the alkyl nitrite (20 μs). As will be shown by the kinetics modeling in the *Results* section, the majority of the OH stretch absorption is due to $\text{HOR}\bullet$ or $\text{HOROO}\bullet$ at 20 μs (94% or 98% respectively). Spectra were also recorded at longer times after photolysis (800 μs) in order to determine how the OH stretch peak changed as secondary products formed.

Of particular note is the lower concentration of RONO used for the OH stretch measurements ($[\text{C}_4\text{H}_9\text{ONO}] = 7.1 \times 10^{15} \text{ molec cm}^{-3}$, $[\text{C}_5\text{H}_{11}\text{ONO}] = 8.1 \times 10^{15} \text{ molec cm}^{-3}$) compared to the A-X experiment ($[\text{C}_4\text{H}_9\text{ONO}] = 6.0 \times 10^{14} \text{ molec cm}^{-3}$, see Chapter 10). Alkyl nitrites have a structured absorption for frequencies $>3300 \text{ cm}^{-1}$ ⁴¹ (see the *Results* section for our measured spectrum). By keeping $[\text{RONO}]$ low, we minimize its background absorption, and therefore reduce the noise level of our spectrometer (Chapter 2). There are two key differences between this experiment and the A-X experiment that allow for this reduction in $[\text{RONO}]$. First, alkyl nitrites do not absorb in the near-IR region where the A-X transitions of HOROO• are located, thus allowing us to indiscriminately increase $[\text{RONO}]$. Second, the absorption cross sections of OH stretch peaks^{40, 41} are typically a factor of 10-100 larger than the cross section of the A-X peak for peroxy radicals.^{44, 115, 122, 124, 184, 185} While a decrease in $[\text{RONO}]$ would render the A-X band of HOROO• undetectable, the OH stretch band is strong enough to still allow for detection HOR• or HOROO•.

The relative kinetics experiments were conducted by varying $[\text{O}_2]$ ($0-8 \times 10^{18} \text{ molec cm}^{-3}$) at roughly constant pressure (300–330 torr) and measuring the resulting absorption at a constant frequency (HOC₄H₈OO• at 3662 cm^{-1} , HOC₅H₁₀OO• at 3660 cm^{-1}), over the range 20–60 μs after photolysis (0.5 μs step size). It can be observed that the intensity of the OH stretch peak does not change over the first 100 μs ,³⁰ and likely longer (see *Results* for more details). We can therefore average the absorptions across the entire timing range as a way to “signal average” our absorptions.

The conditions for the three experiments are summarized in Tables 7.2 (*n*-butoxy) and 7.3 (2-pentoxy). Gas flows were measured using the flowmeters discussed in

Chapter 2. The temperature of the gas kinetics cell was taken to be room temperature: no temperature control of any kind was attempted.

Table 7.2. Experimental conditions (gas flows, photolysis parameters, chemical concentrations, and spectrometer performance) for *n*-butoxy experiments

	HOC ₄ H ₈ OO• Spectrum, 300 torr	HOC ₄ H ₈ • Spectrum, 300 torr	Relative rate, 300-330 torr
N ₂ Purge Flow—Left Mirror	550 sccm	550 sccm	550 sccm
N ₂ Purge Flow—Right Mirror	500 sccm	500 sccm	500 sccm
N ₂ Bubbler Flow	48 sccm 171 sccm ^b	48 sccm	48 sccm
N ₂ Dilution Flow	2700 sccm	2700 sccm	0-2700 sccm ^a
O ₂ Flow	400 sccm	0 sccm	0-2700 sccm ^a
Cell Pressure	300 torr 310 torr ^b	270 torr	300 torr
Temperature (room)	293 ± 2 K	293 ± 2 K	293 ± 2 K
Flush Time	25 ms	25 ms	25 ms
Photolysis Window Length	5 cm	5 cm	5 cm
Excimer Energy at 351 nm	160 ± 10 mJ/pulse	160 ± 10 mJ/pulse	160 ± 10 mJ/pulse
% Alkoxy Photolyzed	1.47%	1.47%	1.47%
[C ₄ H ₉ ONO] _{cell}	7.1 × 10 ¹⁵ cm ⁻³ 2.4 × 10 ¹⁶ cm ⁻³ ^b	7.1 × 10 ¹⁵ cm ⁻³	7.1 × 10 ¹⁵ cm ⁻³
[C ₄ H ₉ O•]	1.1 × 10 ¹⁴ cm ⁻³ 3.6 × 10 ¹⁴ cm ⁻³ ^b	1.1 × 10 ¹⁴ cm ⁻³	1.1 × 10 ¹⁴ cm ⁻³
[O ₂]	9.0 × 10 ¹⁷ cm ⁻³ 8.0 × 10 ¹⁸ cm ⁻³ ^b	0 cm ⁻³	(1–8) × 10 ¹⁸ cm ⁻³
Optical Cell Length	52 cm	52 cm	52 cm
1/τ ₀ (3638 cm ⁻¹ , purge only)	1.2 × 10 ⁵ Hz	1.2 × 10 ⁵ Hz	1.2 × 10 ⁵ Hz
1/τ (3670 cm ⁻¹ , all background gases, no C ₄ H ₉ ONO)	1.6 × 10 ⁵ Hz	1.6 × 10 ⁵ Hz	1.6 × 10 ⁵ Hz
1/τ (3670 cm ⁻¹ , all background gases and C ₄ H ₉ ONO)	2.5 × 10 ⁵ Hz 4.9 × 10 ⁵ Hz ^b	2.5 × 10 ⁵ Hz	2.5 × 10 ⁵ Hz
Δτ/τ ^c	0.8%	0.8%	0.8%
Sensitivity (3670 cm ⁻¹ , with C ₄ H ₉ ONO background, 2σ)	6.9 ppm Hz ^{-1/2} 13.6 ppm Hz ^{-1/2} ^b	6.9 ppm Hz ^{-1/2}	6.9 ppm Hz ^{1/2}

a) The sum of O₂ and N₂ dilution flows was kept at 2700 sccm for the relative rate experiments to keep a constant pressure and flush time

b) Increased [RONO] and [O₂] only used for separate experiments. These scans were not averaged into the reported spectrum

c) Δτ/τ reported for averaging 16 ringdown traces per point

Table 7.3. Experimental conditions (gas flows, photolysis parameters, chemical concentrations, and spectrometer performance) for 2-pentoxy experiments

	HOC ₅ H ₁₀ OO• Spectrum, 320 torr	HOC ₅ H ₁₀ • Spectrum, 320 torr	Relative rate, 320 torr
N ₂ Purge Flow—Left Mirror	550 sccm	550 sccm	550 sccm
N ₂ Purge Flow—Right Mirror	500 sccm	500 sccm	500 sccm
N ₂ Bubbler Flow	83 sccm 265 sccm ^b	83 sccm	83 sccm
N ₂ Dilution Flow	2700 sccm	3300 sccm	0-2700 sccm ^a
O ₂ Flow	400 sccm	0 sccm	0-2700 sccm ^a
Cell Pressure	320 torr	320 torr	320 torr
Temperature (room)	293 ± 2 K	293 ± 2 K	293 ± 2 K
Flush Time	25 ms	25 ms	25 ms
Photolysis Window Length	5 cm	5 cm	5 cm
Excimer Energy at 351 nm	170 ± 10 mJ/pulse	170 ± 10 mJ/pulse	170 ± 10 mJ/pulse
% Alkoxy Photolyzed	1.19%	1.19%	1.19%
[C ₅ H ₁₁ ONO] _{cell}	8.1 × 10 ¹⁵ cm ⁻³ 2.5 × 10 ¹⁶ cm ⁻³ ^b	8.1 × 10 ¹⁵ cm ⁻³	8.1 × 10 ¹⁵ cm ⁻³
[C ₅ H ₁₁ O•]	9.6 × 10 ¹³ cm ⁻³ 3.0 × 10 ¹⁴ cm ⁻³ ^b	9.6 × 10 ¹³ cm ⁻³	9.6 × 10 ¹³ cm ⁻³
[O ₂]	9.5 × 10 ¹⁷ cm ⁻³	0 cm ⁻³	(1–8) × 10 ¹⁸ cm ⁻³
Optical Cell Length	52 cm	52 cm	52 cm
1/τ ₀ (3638 cm ⁻¹ , purge only)	1.2 × 10 ⁵ Hz	1.2 × 10 ⁵ Hz	1.2 × 10 ⁵ Hz
1/τ (3638 cm ⁻¹ , all background gases, no C ₅ H ₁₁ ONO)	1.4 × 10 ⁵ Hz	1.4 × 10 ⁵ Hz	1.4 × 10 ⁵ Hz
1/τ (3660 cm ⁻¹ , all background gases and C ₅ H ₁₁ ONO)	2.5 × 10 ⁵ Hz 5.5 × 10 ⁵ Hz ^b	2.5 × 10 ⁵ Hz	2.5 × 10 ⁵ Hz
Δτ/τ ^c	0.3%	0.3%	0.3%
Sensitivity (3660 cm ⁻¹ , with C ₅ H ₁₁ ONO background, 2σ)	3.3 ppm Hz ^{-1/2} 7.2 ppm Hz ^{-1/2} ^b	3.3 ppm Hz ^{-1/2}	3.3 ppm Hz ^{-1/2}

a) The sum of O₂ and N₂ dilution flows was kept at 2700 sccm for the relative rate experiments to keep a constant pressure and flush time

b) Increased [RONO] only used for a separate experiment. This scan was not averaged into the reported spectrum

c) Δτ/τ reported for averaging 16 ringdown traces per point

We can calculate the cell flush time, [RONO], and [RO•] based on the experimental parameters in Tables 7.2 and 7.3. Derivations of these equations are presented in Chapter 8 (reanalysis of previous experiments); therefore, only the final results are presented here. The flush time is defined as the amount of time to remove the chemicals within the photolysis length from the ringdown cavity, and is calculated from Equation 7.13:

$$t_{flush} = \left(\frac{V_{in-out}}{\sum_{flush} f_i} \right) \times \left(\frac{p_{cell}}{p_{st}} \right), \quad (7.13)$$

where t_{flush} is the flush time for the chemical sample, V_{in-out} is the volume between the inlet for butyl nitrite and vacuum outlet ($V_{in-out} = 3.93 \text{ cm}^3$ for the cell used in this experiment), $\sum_{flush} f_i$ is the total flow rate of gases in the direction of flushing (in sccm), p_{cell} is the pressure in the CRDS cell, and p_{st} is the standard pressure (760 torr).

[RONO] in the CRDS cell is determined by the vapor pressure of the alkyl nitrite and the dilution of the butyl nitrite carrier gas within the CRDS cell, and can be calculated from Equation 7.14:

$$\left(\frac{N}{V} \right)_{RONO,CRDS} = p_{vap} \left(\frac{N/V}{P} \right)_{conv} \left(\frac{T_{bubbler}}{T_{cell}} \right) \left(\frac{f_{bubbler}}{\sum f_i} \right), \quad (7.14)$$

where $\left(\frac{N}{V} \right)_{RONO,CRDS}$ is the concentration of butyl nitrite in the CRDS cell, p_{vap} is the vapor pressure of RONO in the bubbler, $T_{bubbler}$ is the temperature of the bubbler (273 K),

$\left(\frac{N/V}{P} \right)_{conv}$ is the conversion factor between pressure and number density of a gas

$(3.24 \times 10^{16} \text{ molec cm}^{-3}/\text{torr})$, T_{cell} is the temperature of the gas kinetics cell (293 K), f_{bubbler} is the gas flow through the bubbler, and Σf_i is the sum of all gas flows through the gas kinetics cell. The vapor pressure of $\text{C}_4\text{H}_9\text{ONO}$ (20.3 torr at 273 K) can be computed based on known thermodynamic properties ($\Delta_{\text{vap}}H$, $T_{\text{boil,1atm}}$). No thermodynamic data exist for 2-pentyl nitrite in the literature; thus, we relied on our measurements of $p_{\text{vap}}(T)$ (see the *Results* section) to obtain the vapor pressure of $\text{C}_5\text{H}_{11}\text{ONO}$ (13.5 torr at 273 K).

The fraction of RONO that is photolyzed can be calculated from Equation 7.15:

$$\%_{\text{photolysis}} = \frac{\left(\frac{P_{\text{excimer}}}{A_{\text{meter}}} \right) \left(\frac{\lambda}{hc} \right) (\sigma_{\text{RONO},\lambda}) (X) \left(\frac{A_{\text{UV,laser}}}{A_{\text{UV,CRDS}}} \right)}{F_{\text{excimer}}}, \quad (7.15)$$

where $\%_{\text{photolysis}}$ is the fraction of RONO that is photolyzed, $(P_{\text{excimer}}/A_{\text{meter}})$ is the power per unit area of the UV light (read directly from the power meter), F_{excimer} is the rep rate of the excimer laser (10 Hz), h is Planck's constant, c is the speed of light, λ is the wavelength of the excimer light (351 nm), $\sigma_{\text{RONO},\lambda}$ is the absorption cross section of RONO at the excimer wavelength ($8 \times 10^{-20} \text{ cm}^2$ at 351 nm for *n*-butyl nitrite, $6 \times 10^{-20} \text{ cm}^2$ for 2-pentyl nitrite), X is the quantum yield for photolysis (taken to be 1), $A_{\text{UV,laser}}$ is the area of excimer beam measured at the excimer laser output, and $A_{\text{UV,CRDS}}$ is the area of excimer beam measured at the CRDS cell. For these experiments, $\frac{A_{\text{UV,laser}}}{A_{\text{UV,CRDS}}} = 2$.

Results

We present the results of this study in four parts. First, we discuss the chemistry relevant to our experiment following photolysis of the alkyl nitrite. Within 20 μs , we show that the majority of product being detected are the primary isomerization products,

HOR• ($[O_2] = 0$) or HOROO• (in the presence of O_2). Second, the OH stretch spectra of HOR• and HOROO• are shown at a constant time after photolysis (20 μ s) and a single starting alkoxy concentration ($[C_4H_9O\bullet] = 1.1 \times 10^{14}$ molec cm^{-3} , $[C_5H_{11}O\bullet] = 9.6 \times 10^{13}$ molec cm^{-3}). The OH stretches for δ -HOC₄H₈• and δ -HOC₄H₈OO• are located at 3675 cm^{-1} , while the OH stretches for δ -HO-1-C₅H₁₀• and δ -HO-1-C₅H₁₀OO• are located at 3660 cm^{-1} . We observe differences in peak intensity and shape between HOR• and HOROO• for both the butoxy and pentoxy systems. Third, we present the observed OH stretch spectra at longer times after alkoxy formation (800 μ s vs 20 μ s) and higher starting radical concentrations ($[RO\bullet] = 3 \times 10^{14}$ molec cm^{-3} vs 1×10^{14} molec cm^{-3}) to compare the band shapes of pure HOROO• and a mixture of HOROO• and secondary products. Fourth, we report the relative rate k_{isom}/k_{O_2} by using the newly measured OH stretch spectra of HOC₄H₈OO• and HOC₅H₁₀OO• to obtain A_0/A as a function of $[O_2]$. The relative rate obtained with our newly measured band is in agreement with all of the available data: previous literature,^{146, 148, 153-158} the reanalysis of the previous OH stretch experiment (Chapter 8), and the A-X experiment (Chapter 10). Finally, we present the analysis of our 2-pentyl nitrite sample: FTIR spectra, purity, vapor pressure measurements, and derived thermodynamic parameters.

Chemistry

Photolysis of the alkyl nitrites in the UV leads to prompt dissociation, with a typical reaction enthalpy of 40 kcal mol⁻¹.¹⁸⁶



For photolysis at 351 nm, the fragments contain 40 kcal mol^{-1} of available energy. The observations by Bruhlmann et al.¹⁸⁷ and Mestdagh et al.¹⁸⁸ of anisotropic product angular distributions in the photolysis of alkyl nitrites indicates that products are formed on timescales less than a rotational period ($<1 \text{ ps}$). $\text{RO}\cdot$ and NO are formed almost exclusively, most likely on the excited RONO electronic surface, with a minor channel leading to OH production.¹⁸⁹ If we assume that the quantum yield for dissociation is $\phi_{7.16} = 1$, then for our laser fluence ($2 \times 10^{17} \text{ photons cm}^{-2}$ at 351 nm), we expect $[\text{C}_4\text{H}_9\text{O}\cdot]_0 = 1 \times 10^{14} \text{ molec cm}^{-3}$. At 300 torr, vibrational relaxation will lead to thermal equilibrium on timescales $\ll 1 \text{ }\mu\text{s}$. Based on rate constants from the literature, isomerization for *n*-butoxy and 2-pentoxy radicals is expected to occur on time scales of $4 \text{ }\mu\text{s}$ ($k_{\text{isom}} = 2.5 \times 10^5 \text{ s}^{-1}$),²⁸



In the absence of O_2 , a small fraction of $\text{HOR}\cdot$ will undergo self-recombination, with lifetime $200 \text{ }\mu\text{s}$ ($k = 5 \times 10^{-11} \text{ cm}^3 \text{ molec}^{-1} \text{ s}^{-1}$).¹¹⁷

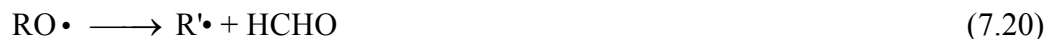


In the presence of O_2 , the hydroxy-alkyl radicals $\text{HOR}\cdot$ will associate to form peroxy radicals $\text{HOROO}\cdot$ with a rate coefficient of roughly $7 \times 10^{-12} \text{ cm}^3 \text{ molec}^{-1} \text{ s}^{-1}$.²⁷



In most of our spectroscopy experiments, $[\text{O}_2] = 30 \text{ torr}$. Under these conditions, the pseudo-first order lifetime of $\text{HOR}\cdot$ is 150 ns . Thus, all of the $\text{HOR}\cdot$ will have been converted to $\text{HOROO}\cdot$. (Note that for lower $[\text{O}_2]$, $0.1\text{--}1 \text{ torr}$, the lifetime of $\text{HOR}\cdot$ increases to $4\text{--}45 \text{ }\mu\text{s}$, and a mixture of $\text{HOR}\cdot$ and $\text{HOROO}\cdot$ is detected. The consequences of this are explored in Chapter 9)

Decomposition of the alkoxy radicals occurs on timescales of 2 ms for *n*-butoxy ($k_{\text{decomp}} = 600 \text{ s}^{-1}$) and 50 μs for 2-pentoxy ($k_{\text{decomp}} = 2 \times 10^4 \text{ s}^{-1}$).¹¹⁷



The alkoxy radicals can also recombine with background and product NO to reform the alkyl nitrite. For our $[\text{NO}] = 10^{14} \text{ molec cm}^{-3}$, this reaction occurs on time scales of 300 μs ($k_{\text{NO}} \times [\text{NO}] = 3000 \text{ s}^{-1}$).³²



There are two concerns regarding secondary chemistry in our experiment. First, any side reactions of the alkoxy radical itself will have an impact on the initial $[\text{RO}\cdot]$ present, affecting both band strength and relative kinetics measurements. Second, hydrogen abstraction by $\text{RO}\cdot$, $\text{HOR}\cdot$, or $\text{HOROO}\cdot$ will lead to different species that contain hydroxyl groups. These species may have different ν_1 bands than $\text{HOR}\cdot$ or $\text{HOROO}\cdot$, and will cause interference in our reported spectra.

First, consider the reactions of the alkoxy radical itself. For our conditions, $[\text{RO}\cdot] = [\text{NO}] = 1 \times 10^{14} \text{ molec cm}^{-3}$. Recombination reactions of $\text{RO}\cdot$ with $\text{RO}\cdot$ or NO ,



are approximately two orders of magnitude slower than isomerization ($k_{\text{NO}} \times [\text{NO}] = 3000 \text{ s}^{-1}$).³² Thus, Reactions 7.5–7.11 will still be the dominant fate of the alkoxy radicals. The overall effect of Reactions 7.22 and 7.23 will be minor. Reaction 7.22 will be especially unimportant due to its quadratic dependence on $[\text{RO}\cdot]$.

We next consider reactions of $\text{RO}\cdot$, $\text{HOR}\cdot$, and $\text{HOROO}\cdot$ that could lead to other products with hydroxyl groups. Continuing our analysis of $\text{RO}\cdot$, we note that alkoxy

radicals could abstract a hydrogen from RONO to form an alcohol (ROH, Reaction 7.24). Furthermore, HOR• could also abstract a hydrogen from RONO to form an alcohol (Reaction 7.25), or HOROO• could form a hydroxyalkylhydroperoxide (HOROOH, Reaction 7.26)



Analogous rate constants ($\text{R}\cdot + \text{R}$, $\text{R}\cdot + \text{ROH}$, $\text{RO}_2\cdot + \text{R}$, $\text{RO}_2\cdot + \text{ROH}$, $\text{RO}\cdot + \text{R}$) for $\text{R} = (\text{CH}_2, \text{C}_2\text{H}_4)$ are in the range 10^{-22} – 10^{-18} $\text{cm}^3 \text{ molec}^{-1} \text{ s}^{-1}$.¹¹⁷ For $[\text{RONO}] = 10^{16}$ molec cm^{-3} , the lifetime of these reactions would be 10^2 – 10^6 s. We conclude that hydrogen abstraction is unimportant over the timescale 20 μs .

Next, we consider whether HOR• or HOROO• are removed through other (nonhydrogen abstraction) mechanisms. First, consider the fate of HOR• radicals in the absence of O₂: self-recombination or recombination with NO.



If we assume that the HOR• + HOR• recombination reactions are in the high pressure limit with rate constant 5×10^{-11} $\text{cm}^3 \text{ molec}^{-1} \text{ s}^{-1}$, a rate constant similar to both HOCH₂• self-reaction and HOC₂H₄• self-reaction,¹¹⁷ then the initial lifetime for Reaction 7.27 is 200 μs . The rate constant for Reaction 7.28 is unknown: analogous reactions have rate constants ranging from 6×10^{-14} $\text{cm}^3 \text{ molec}^{-1} \text{ s}^{-1}$ ($\text{C}_3\text{H}_7\cdot + \text{NO}$) to 2×10^{-11} $\text{cm}^3 \text{ molec}^{-1} \text{ s}^{-1}$ ($\text{HOCH}_2\cdot + \text{NO}$). For $[\text{NO}] = 1 \times 10^{14}$ molec cm^{-3} , we obtain $k_{28} \times [\text{NO}] = (6\text{--}2000) \text{ s}^{-1}$, or lifetimes of (0.5–170) ms. Regardless of the exact value of the rate

constant for $\text{HOR}\cdot + \text{NO}$, the reaction is at least two orders of magnitude less important than isomerization, and $[\text{HORNO}]$ can be considered negligible at 20 μs . Thus, at 20 μs , most (>90%) of the primary products will be $\text{HOR}\cdot$ monomers, with a small fraction recombining to form HORROH . The other products of Reaction 7.27 include hydrogen abstraction to form ROH and hydroxyl-butenes, but similar reaction channels in $\text{HOCH}_2\cdot$ or $\text{HOC}_2\text{H}_4\cdot$ self-reactions have a rate constant less than 10% of the overall rate for Reaction 7.27.¹¹⁷ Thus, ROH formation by $\text{HOR}\cdot$ hydrogen abstraction is negligible at 20 μs . The reaction rate for recombination with NO (Reaction 7.28) is too small to expect an appreciable contribution from HORNO . Similarly, a negligible amount of $\text{HOR}\cdot$ may have undergone hydrogen abstraction by NO to form butanol and a hydroxy-butene. The end result is that besides the small fraction of $\text{HOR}\cdot$ that recombines to form HORROH , no other reactions convert $\text{HOR}\cdot$ to other hydroxyl containing products over the timescale of our experiment (20 μs).

Finally, consider whether $\text{HORO}\cdot$ could be removed by other mechanisms. Further reaction of $\text{HORO}\cdot$ with NO will give a hydroxyalkoxy ($\text{HORO}\cdot$) and NO_2 (Reaction 7.29), with a rate coefficient of approximately $9 \times 10^{-12} \text{ cm}^3 \text{ molec}^{-1} \text{ s}^{-1}$. A minor association channel also exists, giving the hydroxyalkylnitrate HORONO_2 (Reaction 7.30), with a rate coefficient of approximately $4 \times 10^{-13} \text{ cm}^3 \text{ molec}^{-1} \text{ s}^{-1}$.¹¹⁸



At the low NO concentrations generated from the photolysis of precursor ($1 \times 10^{14} \text{ molec cm}^{-3}$), the pseudo-first-order lifetime of $\text{HORO}\cdot$ for reaction with NO is on the order of 1 ms: too long to be of importance. Assuming that the rate constant for the

HOROO• self-reaction is comparable to that for *n*-C₄H₉OO• self-reaction (4×10^{-13} cm³ molec⁻¹ s⁻¹),¹⁹⁰ no appreciable reaction of HOROO• will occur in less than 1 ms.

In theory, HOROO• could also abstract hydrogen through self-reaction:



The analogous rate constants (RO₂• + R, RO₂• + ROH) are on the order 10⁻²²–10⁻¹⁷ cm³ molec⁻¹ s⁻¹.¹¹⁷ For [HOROO•] = 10¹⁴ molec cm⁻³, the initial lifetime for Reaction 7.31 would be a minimum of 500 s. We reach a similar conclusion as the HOR• system: HOROO• does not react away to form other hydroxyl containing products over 20 μs. In the case of HOROO•, we do not have a contribution from recombination.

Based on all of the chemistry presented above, we expect that at 20 μs, only primary alkoxy chemistry (isomerization, reaction with O₂, decomposition, dimerization of HOR• in the absence of O₂, and formation of HOROO• in the presence of O₂) will contribute significantly to our experiment. Secondary reactions of RO•, HOR•, and HOROO• will not lead to spectral interference.

Kinetics Modeling

To further confirm that secondary chemistry effects are minimal, we constructed a kinetics model using rate constants available in the literature^{27, 117, 118} with the Kintecus kinetics modeling software.¹⁹¹ This kinetics model is one of the main tools used in Chapter 9, and is described in full detail there.

Figure 7.2 shows the simulated fractions of hydroxyl containing species present in our experiment over the range 0–100 μs after generating RO•. The modeled data are for *n*-butoxy, but similar results apply to 2-pentoxy. The conditions used for these

simulations are the same as in our CRDS experiment (Table 7.2). Our model shows that for $[O_2] = 0$, the cavity ringdown spectrum 20 μs after RONO photolysis will be predominantly $\text{HOR}\cdot$ (94%), with minor contributions from the recombination product HORROH (6%). For $[O_2] = 1 \times 10^{18} \text{ molec cm}^{-3}$, the measured spectrum should be >98% $\text{HOROO}\cdot$. At later times, a significant amount of the stable end-product $\text{HOR}'\text{CHO}$ is observed.

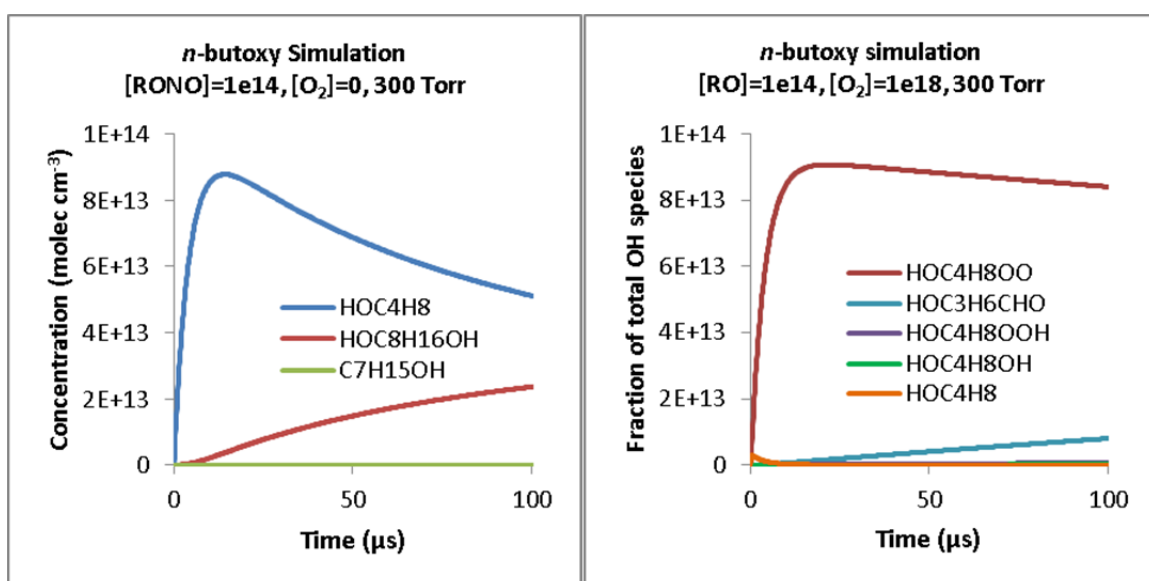


Figure 7.2. Modeled concentrations of $-\text{OH}$ containing species for n -butoxy chemistry, for $[O_2] = 0$ torr (left), and $[O_2] = 1 \times 10^{18} \text{ molec cm}^{-3}$ (right). Experimental conditions are the same as in Table 7.2. At 20 μs , we expect our spectra to be predominantly $\text{HOR}\cdot$ (94%, $[O_2] = 0$) or $\text{HOROO}\cdot$ (98%, $[O_2] = 1 \times 10^{18} \text{ molec cm}^{-3}$).

OH Stretch Spectra of $\delta\text{-HOC}_4\text{H}_8\cdot$, $\delta\text{-HOC}_4\text{H}_8\text{OO}\cdot$, $\delta\text{-HO-1-C}_5\text{H}_{10}\cdot$, and $\delta\text{-HO-1-C}_5\text{H}_{10}\text{OO}\cdot$

Figures 7.3–7.6 show a series of infrared spectra obtained following the photolysis of n -butyl nitrite or 2-pentyl nitrite precursors. All spectra shown were taken with a photolysis-probe delay of 20 μs , with a 0.2 cm^{-1} step size. The spectra presented in Figure 7.3 are unsubtracted (i.e., the mirror reflectivity and absorption by the background

gases have not been subtracted out). Figures 7.4–7.6 have had the background spectra in the absence of photolysis (excimer off) subtracted.

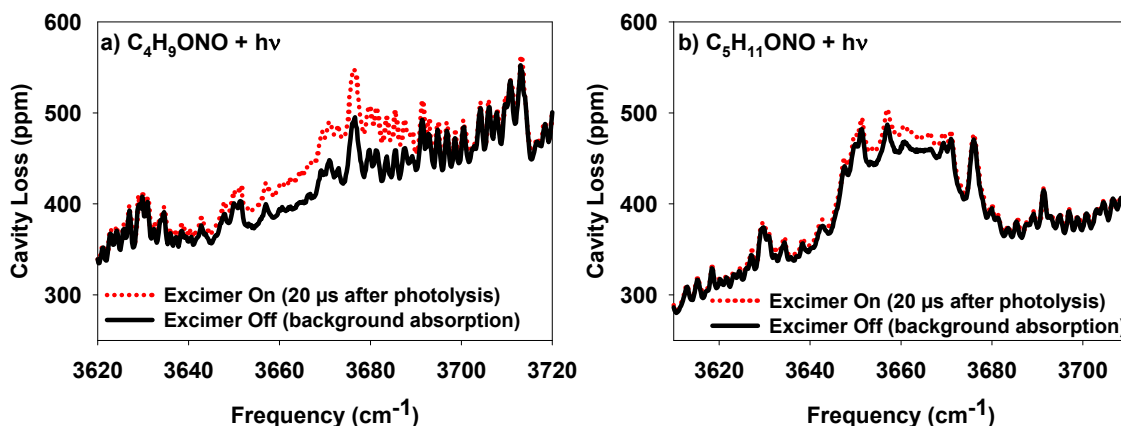


Figure 7.3. Cavity loss (mirror reflectivity plus absorption) of the precursor chemicals (excimer off) and the photolysis products (excimer on) in the mid-IR for *n*-butyl nitrite (a, 300 torr) and 2-pentyl nitrite (b, 315 torr). All spectra were taken at room temperature (295 ± 2 K) and $[\text{O}_2] = 1 \times 10^{18}$ molec cm⁻³, 0.2 cm⁻¹ between data points. The alkyl nitrite absorptions show considerable structure across the entire region. The large peak in the 2-pentyl nitrite spectrum centered at 3660 cm⁻¹ is due to residual 2-pentanol. Additional absorption features are observed following photolysis of the alkyl nitrite. Reprinted with permission from Sprague et al.³¹ Copyright 2012 American Chemical Society.

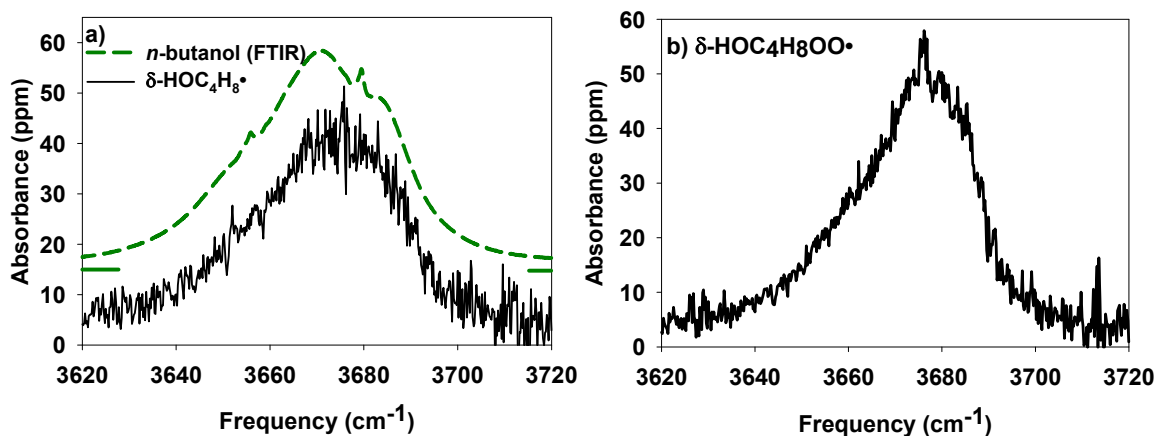


Figure 7.4. ν_1 (OH stretch) spectra of the isomerization of products of *n*-butoxy, in the absence ($\delta\text{-HOC}_4\text{H}_8\bullet$, a) and presence of O_2 ($\delta\text{-HOC}_4\text{H}_8\text{OO}\bullet$, b, $[\text{O}_2] = 9 \times 10^{17}$ molec cm^{-3}). Spectra were recorded at 295 K, 300 torr, 0.2 cm^{-1} between data points, 20 μs after photolysis of *n*-butyl nitrite, $[\text{RONO}] = 7 \times 10^{15}$ molec cm^{-3} , with a 1.5% photolysis ratio. The $\delta\text{-HOC}_4\text{H}_8\bullet$ spectrum was signal averaged for 4.8 s per point, while the $\delta\text{-HOC}_4\text{H}_8\text{OO}\bullet$ spectrum was signal averaged for 8.0 s per point. Both spectra are similar in position and shape to the FTIR spectrum of *n*-butanol (a, shown in green).⁴⁰ Assuming an isomerization rate constant $k_{\text{isom}} = 2.4 \times 10^5 \text{ s}^{-1}$, we predict that in the absence of O_2 , 94% of the product being measured is $\text{HOC}_4\text{H}_8\bullet$, and 6% is its dimer, $\text{HOC}_8\text{H}_{16}\text{OH}$. In the presence of O_2 , we predict that 98% of the product being measured is $\text{HOC}_4\text{H}_8\text{OO}\bullet$ and 2% are other secondary products. Reprinted with permission from Sprague et al.³¹ Copyright 2012 American Chemical Society.

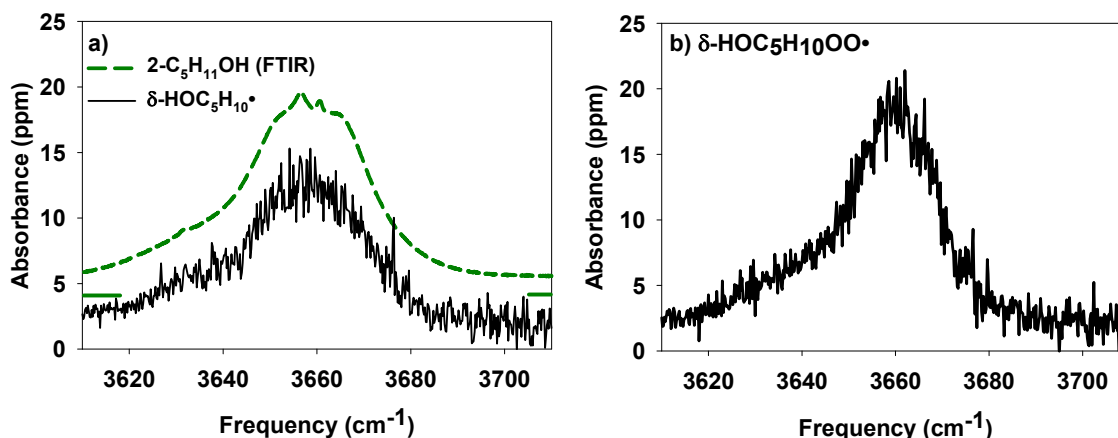


Figure 7.5. ν_1 (OH stretch) spectra of the isomerization of products of 2-pentoxyl, in the absence (δ -HO-1-C₅H₁₀•, a) and presence of O₂ (δ -HO-1-C₅H₁₀OO•, b, [O₂] = 1×10^{18} molec cm⁻³). Spectra were recorded at 295 K, 315 torr, 0.2 cm⁻¹ between data points, 20 μ s after photolysis of 2-pentyl nitrite, [RONO] = 8×10^{15} molec cm⁻³. The photolysis ratio is not well known: if the UV cross section of 2-pentyl nitrite is taken to be 0.75 times that of *n*-butyl nitrite, then [RO•]₀ = 1×10^{14} molec cm⁻³. The peak intensities suggest that [HOR•]₀ = 5×10^{13} molec cm⁻³. Both the δ -HO-1-C₅H₁₀• and δ -HO-1-C₅H₁₀OO• spectra were signal averaged for 11.2 s per point. Both spectra are similar in position and shape to the FTIR spectrum of 2-pentanol (a, shown in green).⁴⁰ Assuming an isomerization rate constant $k_{\text{isom}} = 2.4 \times 10^5$ s⁻¹, we predict that in the absence of O₂, 94% of the product being measured is δ -HO-1-C₅H₁₀•, and 6% is its dimer, HOC₁₀H₂₀OH. In the presence of O₂, we predict that 98% of the product being measured is δ -HO-1-C₅H₁₀OO• and 2% are other secondary products. Reprinted with permission from Sprague et al.³¹ Copyright 2012 American Chemical Society.

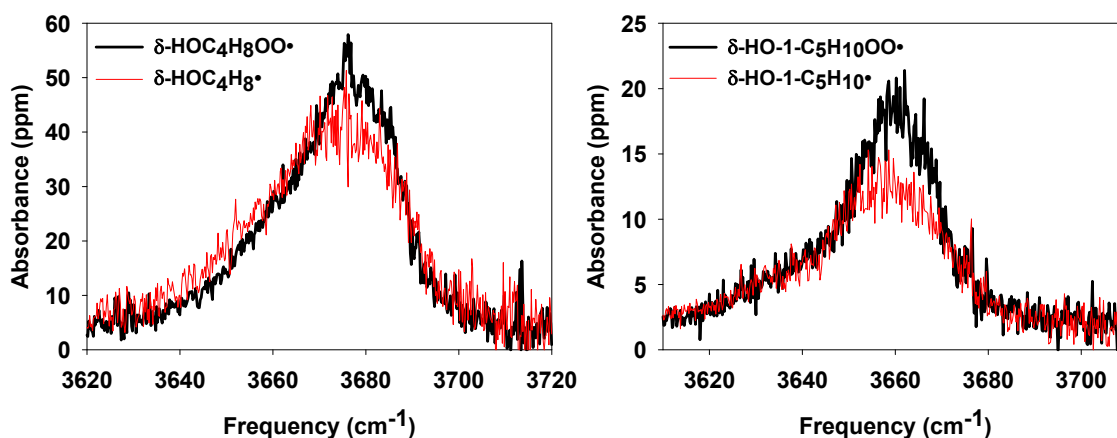


Figure 7.6. Overlaid spectra of δ -HOR• (red) and δ -HOROO• (black) for R = C₄H₈ (left, [HOROO•]/[HOR•] = 0.95) and R = 1-C₅H₁₀ (right, [HOROO•]/[HOR•] = 0.97). Relative concentrations were calculated assuming $k_{\text{isom}}/k_{\text{O}_2} = 1.7 \times 10^{19} \text{ cm}^{-3}$ (*n*-butoxy) or $3.4 \times 10^{19} \text{ cm}^{-3}$ (2-pentoxy), as determined in Chapter 8. We observe that the ν_1 band of HOROO• is narrower and stronger than HOR• for both systems. Reprinted with permission from Sprague et al.³¹ Copyright 2012 American Chemical Society.

Figure 7.3 shows the background IR spectra of the reactants (excimer off) and the IR spectra of the background plus signal (excimer on) for *n*-butyl nitrite (Figure 7.3a) and 2-pentyl nitrite photolysis (Figure 7.3b). Two species contribute to the background in both spectra: the parent alkyl nitrites (broad, structured absorption across the range 3610–3720 cm⁻¹) and water (sharp features at 3630, 3650, 3670, and 3690 cm⁻¹). In the 2-pentyl nitrite spectrum, an additional broad, structureless absorption from 2-pentanol is observed at 3660 cm⁻¹.

Following photolysis at 351 nm, absorption bands are observed, centered near 3675 cm⁻¹ in the *n*-butyl nitrite spectrum and 3660 cm⁻¹ for the 2-pentyl nitrite spectrum, on top of the background features. Figures 7.4 and 7.5 show the IR spectra of products formed following the generation of two different alkoxy radicals: *n*-butoxy (Figure 7.4), and 2-pentoxy (Figure 7.5), in the absence (Figures 7.4a and 7.5a) and presence (Figures

7.4b, 7.5b) of O₂. Following photolysis of *n*-butyl nitrite and 2-pentyl nitrite, clear peaks are observed in the OH-stretch region, located at 3675 cm⁻¹ for *n*-butyl nitrite, and 3660 cm⁻¹ for 2-pentyl nitrite. These absorption features are broad (FWHM > 30 cm⁻¹) and asymmetric, with more intensity observed to the red of the peak. The width and partial structure of these peaks suggest that multiple conformers contribute to each observed absorption band. Furthermore, the observed peaks are similar in shape and position to the parent alcohols of the alkoxy radicals being studied. In the *n*-butoxy system (Figure 7.4), the observed absorption band is similar to the ν₁ band of *n*-butanol (reference FTIR spectrum shown in green).⁴⁰ Similarly, for the 2-pentoxy system (Figure 7.5), the observed absorption band is similar to the ν₁ band of 2-pentanol.⁴⁰ It should be noted that the absorption bands are somewhat stronger and sharper in the presence of O₂ than in the absence of O₂. Figure 7.6 shows these bands overlaid to illustrate this point. Analogous peaks were not observed following the photolysis of isobutyl nitrite or *tert*-butyl nitrite, as shown in Figure 7.7.

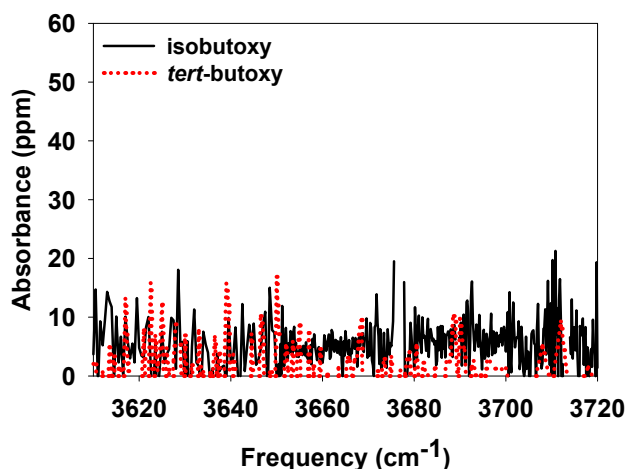


Figure 7.7. Infrared spectra of the products formed from photolysis of isobutyl nitrite and *tert*-butyl nitrite. Spectra were recorded at 295 K, 300 torr, 0.2 cm^{-1} between data points, $20 \mu\text{s}$ after photolysis of the alkyl nitrite, $[\text{RONO}] = 8.1 \times 10^{15} \text{ molec cm}^{-3}$, with a 1.2% photolysis ratio. No absorption features in the ν_1 region are observed, indicating that the products of isobutoxy and *tert*-butoxy chemistry do not contain hydroxyl groups. Reprinted with permission from Sprague et al.³¹ Copyright 2012 American Chemical Society.

We assign the absorption bands presented in Figures 7.4 and 7.5 to the primary alkoxy isomerization products for the following reasons. First, the absorption bands that we observe are similar to the ν_1 (OH stretch) bands of *n*-butanol and 2-pentanol. The primary isomerization products have structures similar to these alcohols (HOR• and HOROO• vs ROH), and we expect similar infrared spectra. Second, we only observe the absorption features for alkoxy radicals that are long enough to undergo a 1,5-hydrogen shift (*n*-butoxy and 2-pentoxy). Neither isobutoxy nor *tert*-butoxy are long enough to isomerize, and thus any absorptions in the *n*-butoxy and 2-pentoxy systems that belonged to isomerization products would be missing. Finally, the arguments presented in the *Chemistry* section indicate that the only significant products that we should be detecting under our experimental conditions are the primary isomerization products. The absence

of any OH stretch bands in the isobutoxy and *tert*-butoxy experiments provides reasonable confirmation that hydrogen abstraction is not leading to significant quantities of parent alcohol (ROH) being detected. We therefore assign the IR spectra in Figures 7.4 and 7.5 to δ -HOC₄H₈• (Figure 7.4a), δ -HOC₄H₈OO• (Figure 7.4b), δ -HO-1-C₅H₁₀• (Figure 7.5a), and δ -HO-1-C₅H₁₀OO• (Figure 7.5b).

The intensity of HOR• is predicted to be similar to the parent alcohol, ROH. We can therefore use the HOR• absorbance to estimate the initial concentration of alkoxy radicals, [RO•]₀. Our quantum chemistry calculations (Chapter 9) confirm that HOR• and the parent alcohol (ROH) have approximately the same absorption cross section. Taking the peak absorption cross section of the HOR• ν_1 peak to be equivalent to the parent alcohols (7.2×10^{-20} cm² molec⁻¹ for *n*-butanol, 6.0×10^{-20} cm² molec⁻¹ for 2-pentanol),⁴⁰ we obtain [HOC₄H₈•]₀ = 1×10^{14} molec cm⁻³ and [HOC₅H₁₀•]₀ = 5×10^{13} molec cm⁻³. These values are consistent with our estimate of the nascent alkoxy product yields (within a factor of 2).

Change in OH Stretch Spectrum with [RO•] and Timing

Spectra were also collected for photolysis-probe delays over the range 10–800 μ s. Figure 7.8 shows the time dependence of the absorbance observed in Figures 7.4 (at 3662 cm⁻¹). We observe that at this frequency, the OH stretch intensity rises with a lifetime of approximately 5 μ s, and reaches a maximum by 20 μ s. Mollner observed that the intensity remains constant for at least 200 μ s,³⁰ indicating that the ν_1 band is a reasonably good way to measure the overall concentration of species with hydroxyl groups. Note that

since the rise time (5 μs) is on the same timescale as our ringdown time (3–7 μs), we cannot use the rise time as a direct measure of the alkoxy isomerization rate constant.

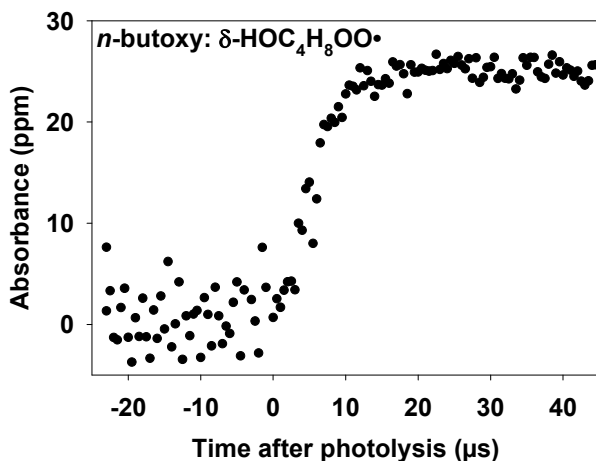


Figure 7.8. Absorbance at 3662 cm^{-1} for *n*-butoxy isomerization as a function of time after *n*-butyl nitrite photolysis. Data were recorded at 295 K, 300 torr, $[\text{O}_2] = 1 \times 10^{18}\text{ molec cm}^{-3}$, $[\text{RONO}] = 7 \times 10^{15}\text{ molec cm}^{-3}$, with a 1.6% photolysis ratio. The absorbance reaches its maximum within 20 μs of photolysis and remains constant thereafter. Reprinted with permission from Sprague et al.³¹ Copyright 2012 American Chemical Society.

Secondary chemistry changes the products being detected at 800 μs . Figure 7.9 shows the expected concentrations of OH containing species across 0–1000 μs based on our kinetics model, for $[\text{O}_2] = 10^{18}\text{ molec cm}^{-3}$, at two different alkoxy concentrations (left – $1 \times 10^{14}\text{ molec cm}^{-3}$, right – $3.7 \times 10^{14}\text{ molec cm}^{-3}$). At 800 μs , only 50% or 21% of the ν_1 band will be due to $\text{HOC}_4\text{H}_8\text{OO}\cdot$. The remaining contributions will be from the stable end-products $\text{HOC}_3\text{H}_6\text{CHO}$ (41% or 59%), $\text{HOC}_4\text{H}_8\text{OOH}$ (8% or 18%), and $\text{HOC}_4\text{H}_8\text{OH}$ (1% or 2%).

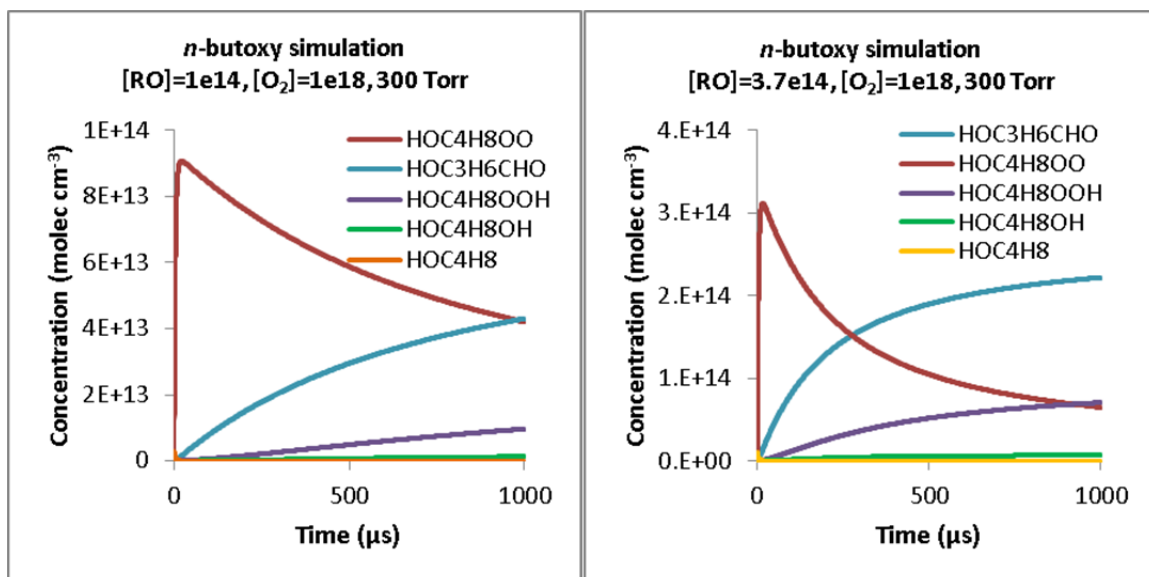


Figure 7.9. Modeled concentrations of $-OH$ containing species for n -butoxy chemistry, $[O_2] = 1 \times 10^{18}$ molec cm^{-3} . The initial alkoxy concentration was either 1×10^{14} molec cm^{-3} (left) or 3.7×10^{14} molec cm^{-3} (right). At 800 μs , we expect our spectra to be a mixture of $HOC_4H_8OO\bullet$ (50% or 21%), HOC_3H_6CHO (41% or 59%), HOC_4H_8OOH (8% or 18%), and HOC_4H_8OH (1% or 2%).

Figure 7.10 shows overlaid spectra comparing the products of alkoxy chemistry at 10 μs , 20 μs , and 800 μs . All spectra were taken at $[O_2] = 1 \times 10^{18}$ molec cm^{-3} . Figure 7.10a compares the 10 μs , 20 μs , and 800 μs spectra for $[RO\bullet] = 1 \times 10^{14}$ molec cm^{-3} . Figure 7.10b compares the 800 μs spectra for $[RO\bullet] = 1 \times 10^{14}$ molec cm^{-3} and 3.7×10^{14} molec cm^{-3} .

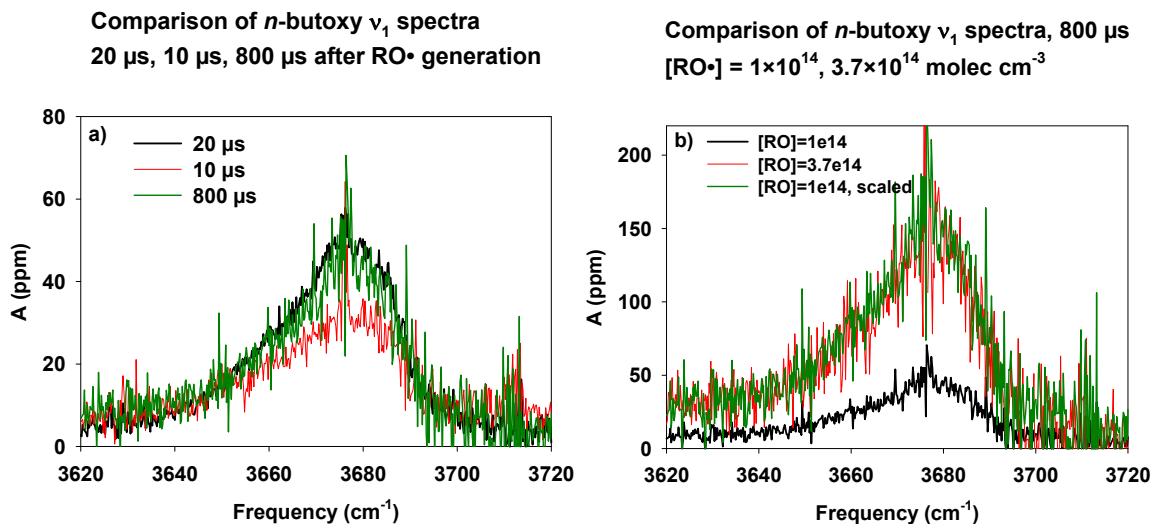


Figure 7.10. ν_1 spectra of *n*-butoxy isomerization products at various conditions. All spectra were taken with $[\text{O}_2] = 9 \times 10^{17} \text{ molec cm}^{-3}$. Figure 7.10a: $[\text{RO}\cdot] = 1 \times 10^{14} \text{ molec cm}^{-3}$, 20 μs (black), 10 μs (red), and 800 μs (green) after photolysis. Figure 7.10b: 800 μs after photolysis, $[\text{RO}\cdot] = 3.7 \times 10^{14} \text{ molec cm}^{-3}$ (red), $1.1 \times 10^{14} \text{ molec cm}^{-3}$ (black, scaled by a factor of 3.4 in green).

First, consider the 10 μs and 20 μs spectra in Figure 7.10a (red and black respectively). Ignoring the sharp spike at 3675 cm^{-1} , the peak absorbance at 10 μs is lower than at 20 μs a factor of 0.7 (33 ppm vs 48 ppm). The 10 μs spectrum (FWHM 35 cm^{-1}) is wider than the 20 μs spectrum (25 cm^{-1}). There are two possibilities to explain these differences, although only one of these is likely. First, isomerization may not be complete after only 10 μs . Given an isomerization lifetime of 5 μs ,^{146, 148, 153-158} we expect 86% of the alkoxy to have isomerized at 10 μs , and 98% at 20 μs , accounting for much of the intensity difference. Second, while it is possible that not all of the $\text{HOR}\cdot$ has been converted to $\text{HOROO}\cdot$ after only 10 μs , this is unlikely. The association of O_2 with $\text{HOR}\cdot$ is very fast ($k_{\text{HOR}+\text{O}_2} \times [\text{O}_2] = 7 \times 10^6 \text{ s}^{-1}$, or lifetime 0.14 μs).²⁷ After 10 μs , 100% of the $\text{HOR}\cdot$ should have been converted to $\text{HOROO}\cdot$.

Next, consider the 20 and 800 μs spectra in Figure 7.10a (black and green respectively). Both spectra have approximately the same shape and intensity, with slight discrepancies near the peak (48 ppm at 20 μs vs 47 ppm at 800 μs) and the baseline at 3620–3640 cm^{-1} (5 ppm at 20 μs vs 8 ppm at 800 μs). The spectra are equivalent in shape and absorbance at frequencies greater than 3680 cm^{-1} . The peak absorbance difference is within the noise of the 800 μs spectrum. The difference in baselines at 3620 cm^{-1} is likely due to absorbance by secondary products. Overall, the spectra are essentially equivalent over the range 3640–3720 cm^{-1} , indicating that the ν_1 band is a very robust measure of the overall number of OH groups in the system.

Third, consider the 800 μs spectra in Figure 7.10b, at low and high $[\text{RO}\cdot]$ (black/green and red respectively). By scaling the low $[\text{RO}\cdot]$ spectrum (black) up to high $[\text{RO}\cdot]$ concentration (green), we observe that the spectrum shape and relative absorbance is invariant to the initial radical concentration. We already have predicted that increasing $[\text{RO}\cdot]$ will change the products being detected at 800 μs (Figure 7.9). Thus, Figure 7.10b provides more evidence that secondary chemistry does not change the properties of the observed ν_1 band.

Finally, consider the sharp spikes in the 10, 20, and 800 μs spectra at 3630, 3650, 3675, and 3710 cm^{-1} . These spikes do not follow the same kinetics as our alkoxy peak; the spikes are largest in the 10 μs spectrum and much lower in the 20 and 800 μs spectra. The spikes likely belong to another chemical species, although we have not identified this species yet.

Determination of the Relative Kinetic Rate $k_{\text{isom}}/k_{\text{O}_2}$

The final goal of the study presented in this chapter was to remeasure $k_{\text{isom}}/k_{\text{O}_2}$ using our new OH stretch spectra of HOROO•, in order to determine whether the previous alkoxy kinetics results (reanalyzed in Chapter 8) obtained an accurate value using the mixed spectrum of HOROO• and HOR'CHO. The results of the previous section showed that the OH stretch spectra of pure HOC₄H₈OO• and a 1:1 mixture of HOC₄H₈OO• and HOC₃H₆CHO were exactly the same. Therefore, we expect our new measurements of $k_{\text{isom}}/k_{\text{O}_2}$ to be within the uncertainty of the previously reported measurements.

Details of how to derive $k_{\text{isom}}/k_{\text{O}_2}$ based on CRDS measurements will be presented with the kinetics analysis (Chapter 8), and only a brief overview is presented here. The relative rate constants of the isomerization channel (Reactions 7.5 and 7.8) and the O₂ channel (Reactions 7.4 and 7.7) can be determined by varying [O₂] and measuring [HOROO•]. By considering only the isomerization and O₂ reaction pathways, the resulting data should fit to Equation 7.32:

$$\frac{A_0}{A} = \frac{k_{\text{O}_2}}{k_{\text{isom}}}[\text{O}_2] + 1, \quad (7.32)$$

where A_0/A is defined as the ratio of absorbances at “[O₂] = 0” and the [O₂] of interest. Because of anomalous behavior in the relative kinetics measurements at low [O₂] (discussed in Chapter 9), “[O₂] = 0” is defined as the y-intercept of the fitted regression line to Equation 7.32, and not the literal absorbance at [O₂] = 0. We then apply a correction factor (Chapter 8) to account for additional reactions of the alkoxy radical. The true $k_{\text{isom}}/k_{\text{O}_2}$ is given by

$$\left(\frac{k_{\text{isom}}}{k_{\text{O}_2}}\right)_{\text{actual}} = \left(\frac{\partial\left(\frac{A_0}{A}\right)}{\partial[\text{O}_2]}\right)^{-1} \times X_{\text{tot}}, \quad (7.33)$$

where $(k_{\text{isom}}/k_{\text{O}_2})_{\text{actual}}$ is the true value of $k_{\text{isom}}/k_{\text{O}_2}$, $\frac{\partial\left(\frac{A_0}{A}\right)}{\partial[\text{O}_2]}$ is the value obtained by fitting to Equation 7.32 (only considering isomerization and reaction with O_2), and X_{tot} is the correction factor that accounts for all other reaction pathways (0.93 ± 0.02 for *n*-butoxy, 0.87 ± 0.04 for 2-pentoxy, 2σ).

Figure 7.11 shows the plots of A_0/A vs $[\text{O}_2]$ for *n*-butoxy (left) and 2-pentoxy (right), measured using the OH stretch spectrum peak. All measurements were made at 3662 cm^{-1} (butoxy) and 3660 cm^{-1} (pentoxy). These points were chosen to obtain a large absorbance while avoiding the sharp spike observed near the $\text{HOC}_4\text{H}_8\text{OO}\cdot$ OH stretch peak at 3675 cm^{-1} . The linear fit for *n*-butoxy is excellent given the low number of data points taken ($R^2 = 96.24\%$), while the fit for 2-pentoxy is somewhat worse ($R^2 = 84.66\%$).

For *n*-butoxy, with 2σ errors, the slope of the plot, $\frac{\partial\left(\frac{A_0}{A}\right)}{\partial[\text{O}_2]}$, is $(4.73 \pm 0.59) \times 10^{-20} \text{ cm}^3$, and the intercept, A_0/A at $[\text{O}_2] = 0$, is (1.00 ± 0.02) . Using $X_{\text{tot}} = 0.93 \pm 0.02$, **the resulting relative kinetic rate constants, $k_{\text{isom}}/k_{\text{O}_2}$, is reported as $(1.96 \pm 0.25) \times 10^{19} \text{ cm}^{-3}$ (2σ error).**

For 2-pentoxy, with 2σ errors, the slope of the plot, $\frac{\partial\left(\frac{A_0}{A}\right)}{\partial[\text{O}_2]}$, is $(2.30 \pm 0.98) \times 10^{-20} \text{ cm}^3$, and the intercept, A_0/A at $[\text{O}_2] = 0$, is (1.00 ± 0.04) . Using X_{tot}

$= 0.87 \pm 0.04$, the resulting relative kinetic rate constants, $k_{\text{isom}}/k_{\text{O}_2}$, is reported as $(3.78 \pm 1.62) \times 10^{19} \text{ cm}^{-3}$ (2σ error).

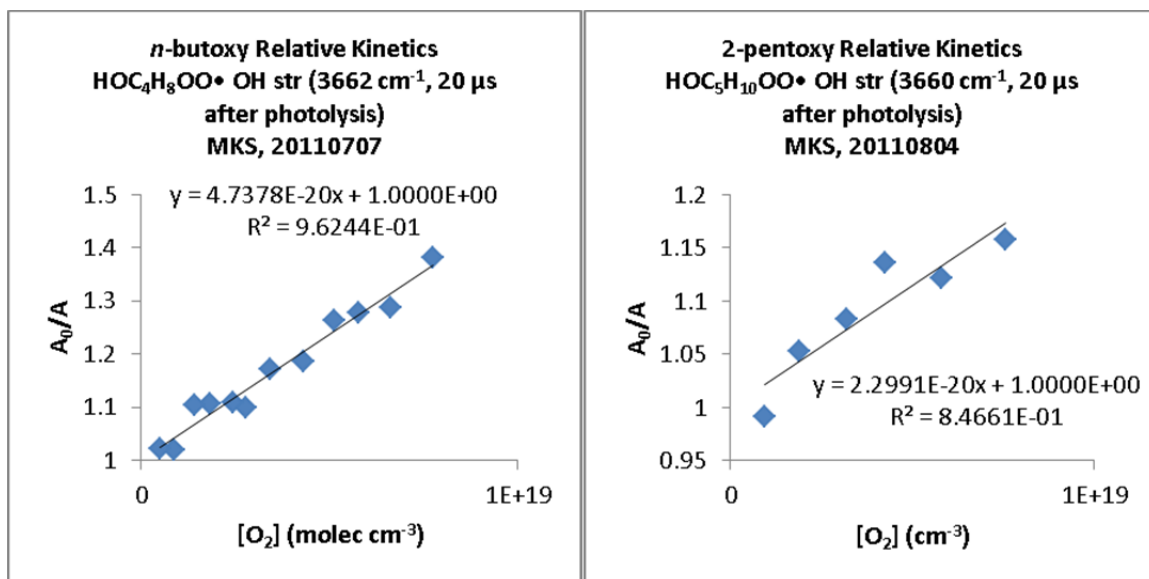


Figure 7.11. Plot of A_0/A vs $[\text{O}_2]$ for *n*-butoxy (left) and 2-pentoxy (right), as measured by the OH stretch peaks at 3662 cm^{-1} (shoulder of *n*-butoxy) or 3660 cm^{-1} (peak of 2-pentoxy). A_0/A is a measure of the percent yield of the isomerization channel as compared to the O_2 channel. For *n*-butoxy, the plot has a slope of $(4.73 \pm 0.59) \times 10^{-20} \text{ cm}^3$, and an intercept of (1.00 ± 0.02) . Applying the correction factor of 0.93 ± 0.02 to account for additional reaction pathways, the resulting $k_{\text{isom}}/k_{\text{O}_2}$ value for *n*-butoxy is determined to be $(1.96 \pm 0.25) \times 10^{19} \text{ cm}^{-3}$. For 2-pentoxy, the plot has a slope of $(2.30 \pm 0.98) \times 10^{-20} \text{ cm}^3$, and an intercept of (1.00 ± 0.04) . Applying the correction factor of 0.87 ± 0.04 to account for additional reaction pathways, the resulting $k_{\text{isom}}/k_{\text{O}_2}$ value for 2-pentoxy is determined to be $(3.78 \pm 1.63) \times 10^{19} \text{ cm}^{-3}$. All errors are reported to 2σ .

Table 7.4 contains a summary of the relative rate constants $k_{\text{isom}}/k_{\text{O}_2}$ for *n*-butoxy and 2-pentoxy from our CRDS experiments and the literature. We observe that the preliminary values of $k_{\text{isom}}/k_{\text{O}_2}$ obtained from the spectroscopic bands presented in this chapter are in very good agreement with all of the previous studies in the literature,^{146, 148, 153-158} including the previous CRDS experiments after reanalysis (Chapter 8) and the A-X electronic band (Chapter 10). The larger uncertainty reported for 2-pentoxy relative to *n*-

butoxy is due to two factors: background 2-pentanol absorption that increases our spectrometer noise, and considerably fewer data points used in the linear fit.

Table 7.4. Comparison of relative rate constant determinations $k_{\text{isom}}/k_{\text{O}_2}$ and derived k_{isom} for *n*-butoxy and 2-pentoxy

	$k_{\text{isom}}/k_{\text{O}_2}$ (10^{19} cm^{-3}) ^a	k_{isom} (10^5 s^{-1}) ^b	Molecules detected	Method	<i>P</i> (<i>torr</i>)	Ref
<i>n</i>-butoxy	1.96 ± 0.25	2.7 ± 1.4	δ-hydroxy- <i>n</i> -butyl peroxy	Slow flow, CRDS (OH Str)	330	This work
	1.39 ± 0.47	2.0 ± 1.2	δ-hydroxy- <i>n</i> -butyl peroxy	Slow flow, CRDS (A-X)	330	Chapter 10
	1.69 ± 0.15	2.4 ± 1.2	δ-hydroxy- <i>n</i> -butyl peroxy	Slow flow, CRDS (OH Str)	670	Chapter 8
	2.0 ± 0.4	2.7 ± 1.5	Butyl nitrite, Butanal,	Static, FTIR	700	Cassanelli ¹⁵⁵
	1.5 ± 0.4	2.1 ± 1.2	4-hydroxy butanal	Static, GC	760	Cox ¹⁵⁶
	1.9 ± 0.4	2.7 ± 1.4	Butane, Butanal	Static, FTIR	700	Niki ¹⁴⁸
	2.1 ± 0.5	2.9 ± 1.6	Butyl nitrite, Butanal	Slow flow, GC	760	Cassanelli ¹⁶⁰
	1.8 ± 1.1	2.5 ± 2.0	Butyl nitrite, Butanal	Slow flow, GC	760	Cassanelli ¹⁶⁰
	1.8 ± 0.6	2.5 ± 1.5	Butane, Butanal	Static, FTIR	760	Geiger ¹⁶¹
	0.25 ± 0.19 ^c	0.35 ± 0.20 ^c	Butanal, 4-hydroxy butanal	Fast flow, LIF	38	Hein ¹⁵⁹
	1.6	2.2	OH and NO ₂	Static, GC	740	Carter ¹⁵⁴
	2.1 ± 1.8 ^d	2.9 ± 1.4 ^d		Recommendation	760	IUPAC ¹¹⁸
2-pentoxy	3.78 ± 1.62	3.0	δ-hydroxy- <i>n</i> -pentyl peroxy	Slow flow, CRDS (OH Str)	330	This chapter
	3.37 ± 0.43 ^e	2.7	δ-hydroxy- <i>n</i> -pentyl peroxy	Slow flow, CRDS (OH Str)	670	Chapter 8
	3.1 ^e	2.5 ^e	2-pentanone	Static, GC	700	Atkinson ¹⁴⁵
	0.15	0.12 ^f	Acetone, Acetaldehyde, 2-hexanol	Static, GC	760	Dóbé ¹⁵⁷

a) All uncertainties are 2σ . All studies other than the current work treat all alkoxy reactions besides isomerization and reaction with O₂ as negligible.

b) Computed k_{isom} assuming literature value of $k_{\text{O}_2} = (1.4 \pm 0.7) \times 10^{-14} \text{ cm}^3 \text{ s}^{-1}$ for *n*-butoxy,²⁸ and $k_{\text{O}_2} = 8 \times 10^{-15} \text{ cm}^3 \text{ s}^{-1}$ for 2-pentoxy (no estimate available for the uncertainty).¹⁴²

c) Unlike the other studies, Hein directly measured k_{isom} . In this table, we calculate the ratio $k_{\text{isom}}/k_{\text{O}_2}$ from Hein's measurement using the literature value of k_{O_2} .

d) The IUPAC recommendation for $k_{\text{isom}}/k_{\text{O}_2}$ is computed from their individual recommendations of the isomerization and O₂ reactions

e) The uncertainty on $k_{\text{isom}}/k_{\text{O}_2}$ is reported by Atkinson as a factor of 2.

f) Dóbé's study calculates k_{isom} from the relative rate $k_{\text{isom}}/k_{\text{decomp}}$ and their measured rate $k_{\text{decomp}} = 1.2 \times 10^4 \text{ s}^{-1}$. The $k_{\text{isom}}/k_{\text{O}_2}$ reported in this table uses the literature value of $k_{\text{O}_2} = 8 \times 10^{-15} \text{ cm}^3 \text{ s}^{-1}$ for 2-pentoxy.¹⁴²

Analysis of Our 2-pentyl nitrite Sample

We now turn our attention to the properties of our 2-pentyl nitrite sample: purity, vapor pressure, and thermodynamic properties ($\Delta_{\text{vap}}H$, $T_{\text{boil,1atm}}$) of our sample. To the best of our knowledge, this is the first report of the thermodynamic properties of 2-pentyl nitrite.

The purity of our synthesized 2-pentyl nitrite (after distillation) can be determined through its FTIR spectrum ($1000\text{--}4000\text{ cm}^{-1}$), shown in Figure 7.12 (left: full spectrum, right: zoomed in to show smaller absorption features). The spectrum was recorded on a Nicolet FTIR spectrometer in Paul Wennberg's laboratory (Caltech), $L_{\text{FTIR}}=19\text{ cm}$. 2-pentyl nitrite was introduced to the spectrometer by evacuating the spectrometer cell, then allowing vapor from our sample into the spectrometer cell. Typical pressures in the spectrometer cell were 1-2 torr.

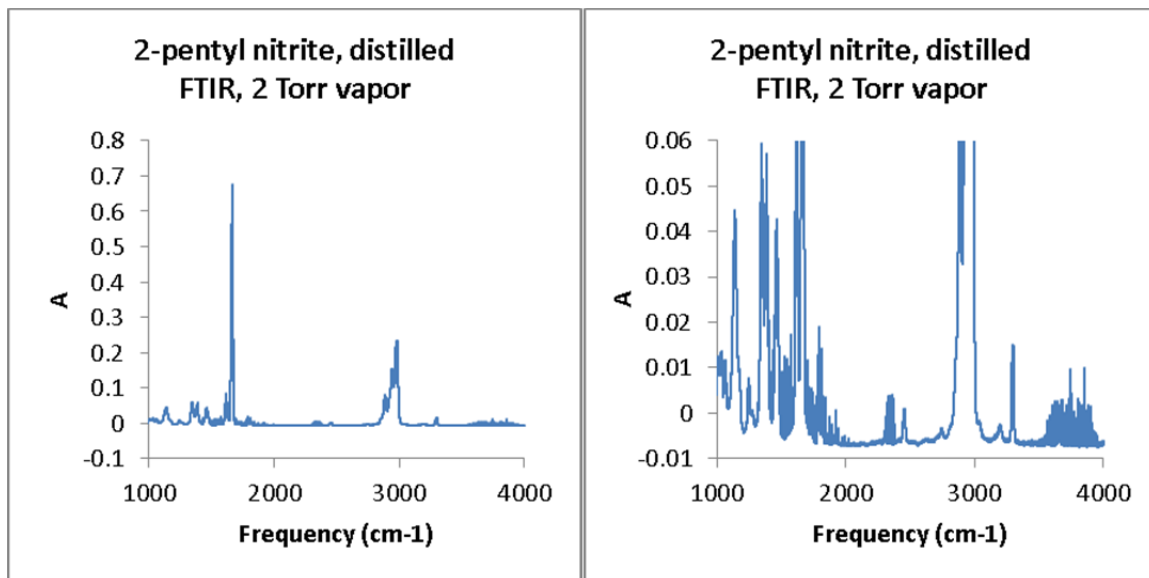


Figure 7.12. FTIR spectrum of our synthesized 2-pentyl nitrite after distillation. The left plot shows the entire spectrum. The right plot zooms in to better show the smaller absorption features. The spectrum was taken by introducing sample vapor to the FTIR. Cell length = 19 cm.

The main contaminants in our 2-pentyl nitrite sample are 2-pentanol (2-C₅H₁₁OH), NO, and H₂O. We use the IR bands of these species to determine their relative concentrations: ON-O stretch of 2-C₅H₁₁ONO (1550–1725 cm⁻¹), NO fundamental vibration (1840–1920 cm⁻¹), H₂O OH stretch modes (3600–3800 cm⁻¹), and the OH stretch of 2-C₅H₁₁OH (3600–3700 cm⁻¹). For H₂O, NO, and 2-C₅H₁₁OH, the individual bands are fit to reference spectra to determine their concentrations.⁴⁰ There is no reference spectrum for 2-C₅H₁₁ONO; thus, the concentration must be computed based on similar reference spectra and theoretical calculations, as described later in this section. Figure 7.13 shows the FTIR bands and fits used to determine the concentrations of each species. Fitting to the reference spectra reveals [H₂O] = 3.5 × 10¹⁵ molec cm⁻³, [NO] = 2 × 10¹⁵ molec cm⁻³, and [NO] = 1.8 × 10¹⁴ molec cm⁻³. A combination of quantum chemistry and reference spectra are required to obtain [2-C₅H₁₁ONO] = 4.8 × 10¹⁶ molec cm⁻³, as shown below.

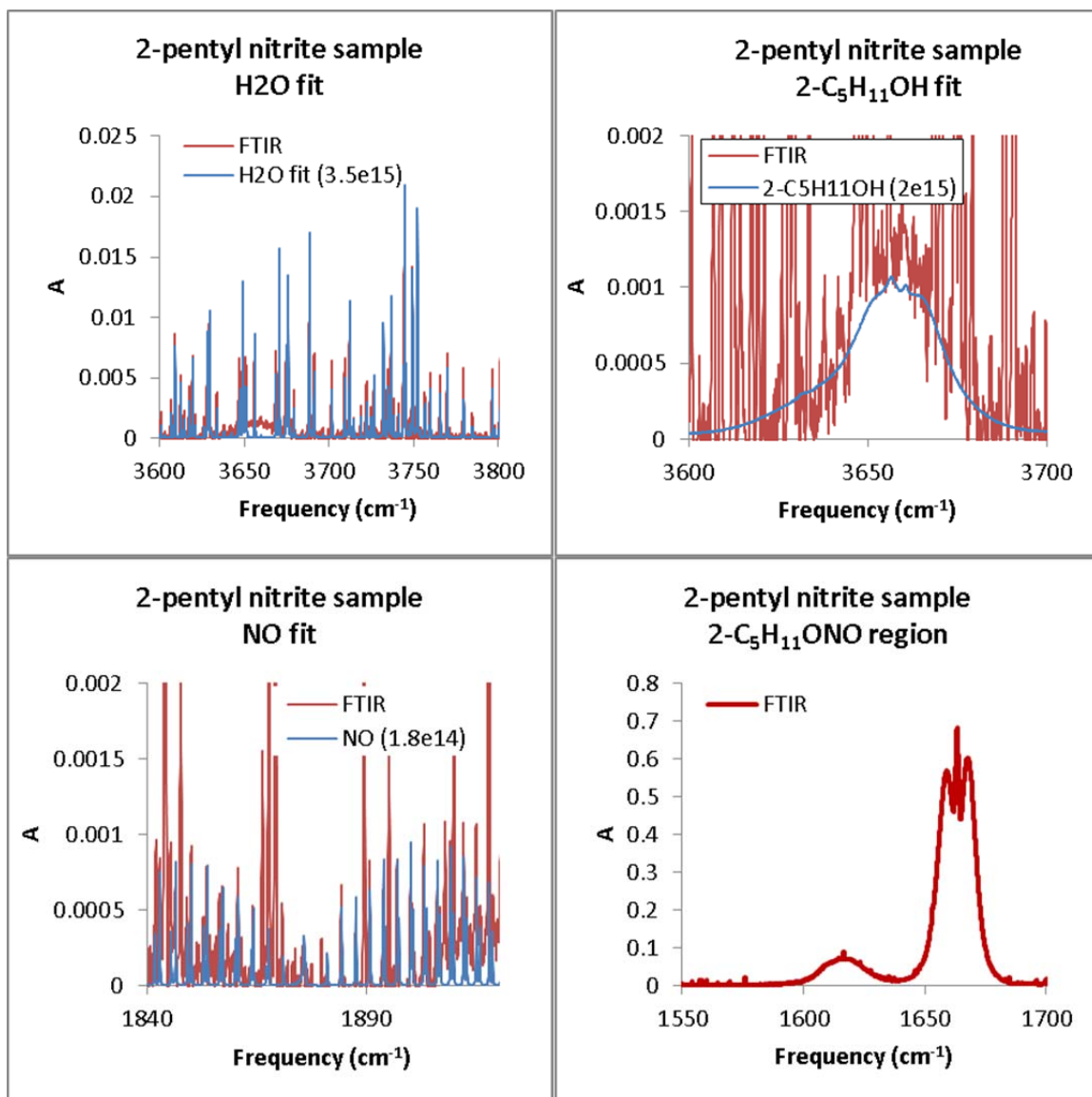


Figure 7.13. Individual FTIR bands for major and minor species in the 2-pentyl nitrite sample. Upper left: H₂O. Upper right: 2-pentanol. Lower left: NO. Lower right: 2-pentyl nitrite. Based on fits to reference spectra, we estimate $[\text{H}_2\text{O}] = 3.5 \times 10^{15} \text{ molec cm}^{-3}$, $[\text{NO}] = 2 \times 10^{15} \text{ molec cm}^{-3}$, and $[\text{NO}] = 1.8 \times 10^{14} \text{ molec cm}^{-3}$. Based on our quantum chemistry analysis, we conclude $[\text{2-C}_5\text{H}_{11}\text{ONO}] = 4.8 \times 10^{16} \text{ molec cm}^{-3}$.

We determine $[\text{2-C}_5\text{H}_{11}\text{ONO}]$ in three steps. First, we obtain the experimentally determined integrated intensities of the ON-O vibrational band from reference spectra of smaller nitrites (CH_3ONO and $\text{C}_2\text{H}_5\text{ONO}$).⁴⁰ Second, we compute relative intensities of relevant alkyl nitrites' ON-O vibrational modes to determine the trend in absorption cross

section. Third, we combine the results of the FTIR spectrum of 2-C₅H₁₁ONO, reference spectrum of smaller RONO, and relative cross sections between alkyl nitrites to obtain [2-C₅H₁₁ONO].

The relevant data needed to compute $\sigma_{2\text{-C}_5\text{H}_{11}\text{ONO}}$, and thus [2-C₅H₁₁ONO], are summarized in Table 7.5. Experimental integrated intensities for CH₃ONO and C₂H₅ONO were taken from reference spectra.⁴⁰ Integrated intensities for all alkyl nitrites were computed at the B3LYP/6-31+G(d,p) level of theory and basis using Gaussian 09W.¹²¹ Intensities were scaled to $I_{\text{calc}}/I_{\text{PNNL}}$ (CH₃ONO) or $I_{\text{calc}}/I_{\text{PNNL}}$ (C₂H₅ONO). The best value for the intensities were taken to be the average of the two scaled intensities.

Table 7.5. Calculated Integrated Intensities for alkyl nitrites, B3LYP/6-31+G(d,p). Intensities were scaled to reference spectra for CH₃ONO and C₂H₅ONO.⁴⁰

	I (PNNL) ^a (km mol ⁻¹)	ν calc (cm ⁻¹)	I calc ^a (km mol ⁻¹)	I , ^a scale to CH ₃ ONO	I , ^a scale to C ₂ H ₅ ONO	I_{best} ^a (km mol ⁻¹)
CH ₃ ONO	171	1686	193	171	175	171
C ₂ H ₅ ONO	182	1679	201	178	182	182
1-C ₃ H ₇ ONO		1678	207	184	188	186
1-C ₄ H ₉ ONO		1678	215	191	195	193
2-C ₅ H ₁₁ ONO		1676	211	187	191	189

a) All intensities converted to base e.

We calculate [2-C₅H₁₁ONO] from Beer's law (Equation 7.34):

$$[\text{C}_5\text{H}_{11}\text{ONO}] = \frac{\int_{1550\text{ cm}^{-1}}^{1700\text{ cm}^{-1}} A_{\text{ON-O}} d\bar{\nu}}{L_{\text{FTIR}} \times \left(\int \sigma_{\text{ON-O,avg}} d\bar{\nu} \right)}, \quad (7.34)$$

where $\int_{1550\text{ cm}^{-1}}^{1700\text{ cm}^{-1}} A_{\text{ON-O}} d\bar{\nu}$ is the observed (FTIR) integrated absorbance, L_{FTIR} is the cell

length (19 cm), and $\int \sigma_{\text{ON-O,avg}} d\bar{\nu}$ is the best value for the integrated intensity (I_{best}) from

Table 7.5. Based on the spectrum in Figure 7.13 and the quantum chemistry data in Table 7.5, we obtain $[2\text{-C}_5\text{H}_{11}\text{ONO}] = 4.8 \times 10^{16} \text{ molec cm}^{-3}$.

Given these calculated concentrations, we obtain the relative concentrations for our contaminants; $[2\text{-C}_5\text{H}_{11}\text{OH}]:[2\text{-C}_5\text{H}_{11}\text{ONO}] = 1:24$, $[\text{NO}]:[2\text{-C}_5\text{H}_{11}\text{ONO}] = 1:240$, and $[\text{H}_2\text{O}]:[2\text{-C}_5\text{H}_{11}\text{ONO}] = 1:14$. Thus, at least 90% of our sample consists of $[2\text{-C}_5\text{H}_{11}\text{ONO}]$.

We next turn our attention to the vapor pressure ($p_{\text{vap}}(T)$) and thermodynamic properties ($\Delta_{\text{vap}}H$, $T_{\text{boil,1atm}}$) of our 2-pentyl nitrite sample. We measured the temperature dependent vapor pressure using the experimental apparatus is shown in Figure 7.14. A 3-necked round-bottomed flask containing 50 mL of 2-pentyl nitrite was immersed in a water bath. The three necks of the flask were fit to a thermometer, two pressure gauges (MKS Baratron and Duniway thermocouple gauge), and an air/vacuum line to control pressure. Data were obtained by cooling the 2-pentyl nitrite sample, removing gas from the 2-pentyl nitrite flask to obtain the pressure of interest, and then slowly heating the water bath until boiling of the 2-pentyl nitrite sample was observed. Nitrogen gas was added to the flask in order to increase the pressure between measurements. Data points below room temperature were taken by using an ice water bath. Data points above room temperature were taken by heating the water bath. Vapor pressure data were taken over the temperature range 276–343 K.

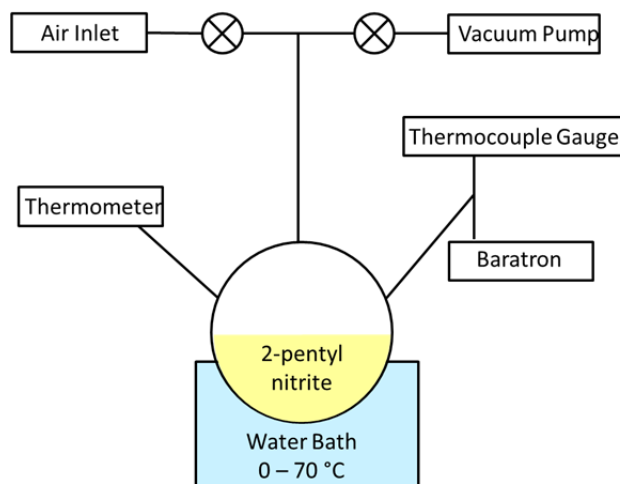


Figure 7.14. Apparatus used to measure the vapor pressure of 2-pentyl nitrite. Reprinted with permission from Sprague et al.³¹ Copyright 2012 American Chemical Society.

Figure 7.15 shows the natural logarithm of the vapor pressure of our sample plotted against the inverse boiling temperature. The plot is linear for temperatures up to 36 °C (309 K, $1000 / T > 3.23 \text{ K}^{-1}$). Above 36 °C, a brown gas evolved from the 2-pentyl nitrite sample, likely corresponding to decomposition of the sample. We observe a kink in the vapor pressure plot, indicating that we may no longer be measuring the properties of 2-pentyl nitrite above 36 °C.

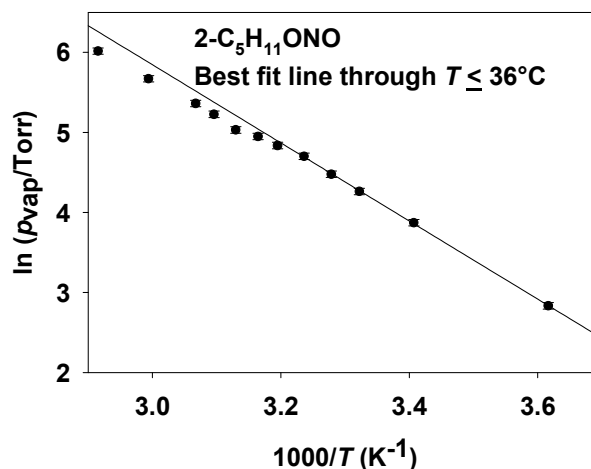


Figure 7.15. Clausius-Clapeyron plot for the 2-pentyl nitrite used for the spectra reported in this work. The data are nonlinear above 36 °C ($1000 / T < 3.23 \text{ K}^{-1}$) due to decomposition of the 2-pentyl nitrite. We report the 2σ uncertainty on each vapor pressure as $\pm 4\%$. The best-fit line to data points at or below 36 °C gives slope = $(-4900 \pm 150) \text{ K}$, intercept = 21 ± 1 . Using these values, $\Delta_{\text{vap}}H = 41 \pm 1 \text{ kJ mol}^{-1}$ and $T_{\text{boil}, 1 \text{ atm}} = (350 \pm 20) \text{ K}$. All uncertainties are reported to 2σ . Reprinted with permission from Sprague et al.³¹ Copyright 2012 American Chemical Society.

The data points prior to decomposition ($T < 36 \text{ °C}$) can be fit to the Clausius-Clapeyron equation:

$$\ln p_{\text{vap}} = \left(-\frac{\Delta_{\text{vap}}H}{R} \right) \left(\frac{1}{T_{\text{vap}}} \right) + \left(\frac{\Delta_{\text{vap}}H}{RT_{\text{boil}}} + \ln p_{\text{atm}} \right), \quad (7.35)$$

where p_{vap} is the vapor pressure at temperature T_{vap} , $\Delta_{\text{vap}}H$ is the enthalpy of vaporization, R is the universal gas constant, and T_{boil} is the boiling point at atmospheric pressure p_{atm} . We assume a 4% uncertainty (2σ) on the vapor pressure data. Including both the error on each vapor pressure data point and overall scatter in the data points, we obtain $\Delta_{\text{vap}}H = 41 \pm 1 \text{ kJ mol}^{-1}$ and $T_{\text{boil}, 1 \text{ atm}} = (350 \pm 20) \text{ K}$. All uncertainties are reported to 2σ .

Although our data fit very well to Equation 7.35, it is important to emphasize that our 2-pentyl nitrite sample was only 90% pure. The major contaminants were water

([H₂O]:[RONO] = 1:14), pentanol (1:24), and NO (1:240). If an azeotrope of 2-pentyl nitrite forms with water or 2-pentanol, then the vapor pressure data may have additional error.

Using our thermodynamic parameters, we determine $p_{\text{vap}}(273 \text{ K})=13.5 \text{ torr}$. We use this value in calculation of [2-C₅H₁₁ONO] for the experiment.

Conclusions

In this chapter, we have reported the first clean ν_1 (OH stretch) vibrational spectra of the primary products of *n*-butoxy and 2-pentoxy isomerization in the absence and presence of oxygen: $\delta\text{-HOC}_4\text{H}_8\bullet$, $\delta\text{-HOC}_4\text{H}_8\text{OO}\bullet$, $\delta\text{-HO-1-C}_5\text{H}_{10}\bullet$, and $\delta\text{-HO-1-C}_5\text{H}_{10}\text{OO}\bullet$. Under our experimental conditions, the recorded spectra are expected to be at least 94% (HOR•) or 98% (HOROO•) primary products. The ν_1 vibrational spectra are similar in shape and intensity to the parent alcohol ROH, with small differences in shape and intensity between HOR• and HOROO•. We observe that the spectra take 20 μs to reach their maximum absorption and remain constant in shape and intensity for at least 800 μs , indicating that secondary products have similar spectra to our HOROO• radicals. We have shown that the ν_1 band can be used for measurement of alkoxy relative kinetics (explored further in Chapter 8). Finally, we make the first report of the vapor pressure and thermodynamic properties of 2-pentyl nitrite.

Acknowledgements

We thank Marissa L. Weichman and Laura A. Mertens for synthesis of the 2-pentyl nitrite used in these experiments and Nathan C. Eddingsaas for assistance with

acquiring the FTIR spectrum of 2-pentyl nitrite. The experiments performed in this chapter were funded under NASA Upper Atmosphere Research Program Grant NNX09AE21G2.